Rene Nauschnig, BSc

# Synthesis and characterization of non-fullerene acceptor materials for the application in organic solar cells

**MASTER THESIS**

In partial fulfilment of the requirements for the academic degree

Diplom-Ingenieur

in the field of study of Technical Chemistry

submitted at

**Graz University of Technology**

Supervisors

Univ.-Prof. Dipl.-Ing. Dr.techn. Gregor Trimmel

Institzte for Chemistry and Technology of Materials

Graz, September 2019

# AFFIDAVIT / EIDESTATTLICHE ERKLÄRUNG

I declare that I have authored this thesis independently, that I have not used other than the declared sources/resources, and that I have explicitly indicated all material which has been quoted either literally or by content from the sources used. The text document uploaded to TUGRAZonline is identical to the present master‘s thesis.

Ich erkläre an Eides statt, dass ich die vorliegende Arbeit selbstständig verfasst, andere als die angegebenen Quellen/Hilfsmittel nicht benutzt, und die den benutzten Quellen wörtlich und inhaltlich entnommenen Stellen als solche kenntlich gemacht habe. Das in TUGRAZonline hochgeladene Textdokument ist mit der vorliegenden Masterarbeit identisch.

Date / Datum

Signature / Unterschrift

# Abstract

Organic photovoltaic based on non-fullerene acceptors are nowadays of great interest. Organic solar cells promise a cheap, non-toxic and easy way of producing electricity out of sun light but still lag behind by other technologies regarding e.g. efficiency or stability. Non-fullerene acceptors display many advantages compared to the very well-studied fullerene acceptors. For example, they are cheaper to synthesize, much easier to modify chemically and in some cases also more stable. Here, non-fullerene acceptors based on a perylene diimide are presented. The perylene core structure was modified by different substituents like Cl-, Br- or Si- compounds with two ethyl (Et) or phenyl (Ph) side groups ($Et_2Si$-, $Ph_2Si$-) and their influence on the solar cell performance was investigated. Every perylene structure contains 2,6-diisopropylphenyl substituents on both imide position to increase the solubility of the compounds. The synthesized structures were characterized by $^1$H-NMR spectroscopy, thermogravimetry, UV-VIS-absorption and emission spectroscopy. The characterisation was assisted by density functional theory (DFT) calculations, to find out the effects of the different substituents on the molecular structure and calculable molecule properties. It is known that an increased dipole moment can cause an increased dielectric permittivity which again is suspected to be beneficial for the solar cell efficiency. Therefore, the optimized structure energy levels and dipole moments were calculated using B3LYP function and a 6-31G* basis sets. Their absorption spectra were also calculated but with time dependent density function theory (TD-DFT) using the same B3LYP function but with a 6-31+G* basis set. Afterwards, the synthesized structures were blended with a polymer donor (PBDB-T) and tested in bulk-heterojunction solar cells. For that an inverted device setup consisting of ZnO as electron transport layer, the active layer of the donor-acceptor blend, $MoO_3$ as hole transport layer and silver as anode, was used. The active layer thickness of the blend was optimized by changing the spin coating speed and concentration of the solution. Furthermore, the influence of light soaking and annealing was investigated. The built solar cells were characterized via J-V-, profilometry-, UV-VIS-absorption, light microscopy and external quantum efficiency measurements. The study shows that the perylene structures with a higher calculated dipole moment also performs better in organic solar cells. DFT calculations show that the introduction of silicon compounds increases the dipole moment. Using molecules, with increased dipole moment and therefore higher dielectric permittivity, as non-fullerene acceptors represents a promising strategy for developing highly efficient organic photovoltaics.

# Kurzfassung

Organische Photovoltaik auf Basis von Non-Fulleren-Akzeptoren ist heutzutage von großem Interesse. Non-Fulleren-Akzeptoren weisen viele Vorteile gegenüber den sehr gut untersuchten Fulleren-Akzeptoren auf. Zum Beispiel sind sie günstiger zu synthetisieren, chemisch viel einfacher zu modifizieren und in einigen Fällen auch stabiler. Organische Solarzellen versprechen einen günstigen, ökologischen und einfachen Weg, Strom aus Sonnenlicht zu erzeugen. Jedoch sind sie aufgrund ihrer noch geringeren Effizienz und Stabilität anderen Photovoltaiktechnologien unterlegen. In dieser Arbeit werden Non-Fulleren-Akzeptoren vorgestellt, die auf einer Perylendiimid-Struktur basieren. Die Perylengrundstruktur wurde durch verschiedene Substituenten wie Cl-, Br-, oder Siliziumverbindungen mit Ethyl (Et) oder Phenyl (Ph) Seitengruppen ($Et_2Si$-, $Ph_2Si$-) modifiziert und deren Einfluss auf die molekularen Eigenschaften untersucht. Jede Perylenstruktur enthält einen 2,6-Diisopropylphenylsubstituenten an beiden Imidposition, um die Löslichkeit der Verbindungen zu erhöhen. Die synthetisierten Strukturen wurden mittels $^1$H-NMR-Spektroskopie, Thermogravimetrie, UV-VIS-Absorptions- und Emissionsspektroskopie charakterisiert. Die Charakterisierung wurde durch dichtefunktionaltheoretische Berechnungen (DFT) ergänzt, um die Auswirkung der unterschiedlichen Substituenten auf die Molekülstruktur und die Moleküleigenschaften zu untersuchen. Es ist bekannt, dass ein erhöhtes Dipolmoment eine erhöhte Dielektrizitätskonstante zufolge haben kann. Von dieser wiederum wird vermutet, dass sie für den Wirkungsgrad der Solarzelle von Vorteil ist. Aus diesem Grund wurden die optimierten Strukturen, Energieniveaus und Dipolmomente unter Verwendung der B3LYP-Funktion und eines 6-31G* Basissatz berechnet. Ihre Absorptionsspektren wurden ebenfalls berechnet, jedoch mittels der Time Dependent-DFT unter Verwendung derselben B3LYP-Funktion kombiniert mit einem 6-31+G* Basissatz. Anschließend wurden die synthetisierten Strukturen mit einem geeigneten Polymerdonor (PBDB-T) vermischt und in Bulk-Heteroübergangssolarzellen getestet. Hierzu wurde ein invertierter Zellenaufbau, bestehend aus ZnO als Elektronentransportschicht, der Aktiv-Schicht bestehend aus dem Donor-Akzeptor-Gemisch, $MoO_3$ als Lochtransportschicht und Silber als Anode verwendet. Die Schichtdicken wurden durch Variieren der Rotationsgeschwindigkeit und der Konzentration optimiert. Darüber hinaus wurde der Einfluss des sogenannten “light-soakings“ und Temperns untersucht. Die gebauten Solarzellen wurden durch J-V-, Profilometrie-, UV-VIS-Absorptions-, Lichtmikroskopie- und externer Quanteneffizienzmessungen charakterisiert. Die Studie zeigt,

dass Perylenstrukturen mit einem höheren berechneten Dipolmoment auch in organischen Solarzellen besser abschneiden. Das Einführen von Siliziumverbindungen in die Grundstruktur steigerte laut DFT Berechnungen effektiv das Dipolmoment. Die Verwendung von Molekülen mit erhöhtem Dipolmoment und daher wahrscheinlich höherer Dielektrizitätskonstante als Nicht-Fulleren-Akzeptoren ist eine vielversprechende Strategie für die Entwicklung hocheffizienter organischer Solarzellen.

# Acknowledgments

First of all, I would like to thank Univ.-Prof. Dipl. Ing. Dr. techn. Gregor Trimmel for giving me the opportunity to do my master thesis on this very interesting topic and also for his profound supervision and support throughout my thesis.

I would also like to thank Stefan Weber who started this project with me and supported me from the beginning. Next I want to thank Matiss Reinfelds for his help and input during my work and the whole working group of Prof. Trimmel for the nice and friendly working environment.

Furthermore, I would like to thank Stefan Stadlbauer and Doris Grössl for their help during the synthesis.

In addition, I would like to thank Michaele Flock for introducing me into the field of computational chemistry and advising me during my calculations.

I also want to thank Josefine Hobisch for doing the thermogravimetric measurements and Petra Kaschnitz for her help with the NMR measurements.

A special thanks goes to my family for supporting me during my whole academic life. In particular I would like to thank my mother Adriana Nauschnig who made it possible and always supported me throughout my studies.

In the end I would like to thank all my friends for their help and for making my student life such a good time.

# List of Abbreviations

| | |
|---|---|
| A | acceptor |
| Accel | acceleration |
| AM | air mass |
| B3LYP | Becke, 3-parameter, Lee–Yang–Parr |
| BDT | 4,8-bis(5-ethylhexylthienyl)-benzo[1,2-b′:4,5-b′]-dithiophene |
| BHJ | bulk-heterojunction |
| BTP-4Cl | 2,2'-((2Z,2'Z)-((12,13-bis(2-ethylhexyl)-3,9-diundecyl-12,13-dihydro-[1,2,5]thiadiazolo[3,4-e]thieno[2",3'':4',5']thieno[2',3':4,5]pyrrolo[3,2-g]thieno[2',3':4,5]thieno[3,2-b]indole-2,10-diyl)bis(methanylylidene))bis(5,6-dichloro-3-oxo-2,3-dihydro-1H-indene-2,1-diylidene))dimalononitrile |
| CB | chlorobenzene |
| CIS | copper-indium-selenide |
| CIGS | copper-indium-gallium-diselenide |
| CSP | concentrating solar power |
| D | donor |
| DCM | dichloromethane |
| DIO | 1,8-Diiodooctane |
| DFT | density function theory |
| DSSC | dye sensitized solar cells |
| $E_B$ | exciton binding energy |
| Eg | band gap [eV] |
| ETL | electron transport layer |
| epPDI | *N*,*N*´-bis(1-ethylpropyl)-3,4,9,10-perylene tetracarboxyl diimide |
| EQE | external quantum efficiency [%] |
| F-DTS | 7,7´-[4,4-bis(2-ethylhexyl)-4*H*-silolo[3,2-*b*:4,5-*b*´]dithiophene-2,6-diyl]bis[6-fluoro-4-(5´-hexyl-[2,2´-bithiophen]-5-yl)benzo[*c*][1,2,5]thiadiazole] |
| FF | fill factor [%] |

| | |
|---|---|
| HOMO | highest occupied molecular orbital |
| HTL | hole transport layer |
| $I_{SC}$ | short circuit current [mA] |
| ITIC | 3,9-bis(2-methylene-(3-(1,1-dicyanomethylene)-indanone))-5,5,11,11-tetrakis(4-hexylphenyl)-dithieno[2,3-d:2’,3’-d’]-s-indaceno[1,2-b:5,6-b’]dithiophene |
| ITO | indium tin oxide |
| $J_{mpp}$ | current density at maximum power point [mA $cm^{-2}$] |
| $J_{SC}$ | short circuit current density [mA $cm^{-2}$] |
| LUMO | lowest unoccupied molecular orbital |
| OPV | organic photovoltaics |
| $V_{mpp}$ | voltage at maximum power point [V] |
| $V_{OC}$ | open circuit voltage [V] |
| P | power |
| P3HT | poly(3-hexylthiophen-2,5-diyl) |
| PBDB-T | Poly[(2,6-(4,8-bis(5-(2-ethylhexyl)thiophen-2-yl)-benzo[1,2-b:4,5-b’]dithiophene))-alt-(5,5-(1’,3’-di-2-thienyl-5’,7’-bis(2-ethylhexyl)benzo[1’,2’-c:4’,5’-c’]dithiophene-4,8-dione)] |
| PBDB-TF | poly[(2,6-(4,8-bis(5-(2-ethylhexyl-3-fluoro)thiophen-2-yl)-benzo[1,2-b:4,5-b’]dithiophene))-alt-(5,5-(1’,3’-di-2-thienyl-5’,7’-bis(2-ethylhexyl)benzo[1’,2’-c:4’,5’-c’]dithiophene-4,8-dione)] |
| PBDTTT-C-T | poly[[4,8-bis[5-(2-ethylhexyl)-2-thienyl]benzo[1,2-b:4,5-b′]dithiophene-2,6-diyl][2-(2-ethyl-1-oxohexyl)thieno[3,4-b]thiophenediyl]] |
| PBDTT-FTTE | poly[4,8-bis(5-(2-ethylhexyl)thiophen-2-yl)benzo[1,2-b;4,5-b′] dithiophene- 2,6-diyl-*alt*-(4-(2-ethylhexyl)-3-fluorothieno[3,4-*b*]thiophene-)-2-carboxylate-2−6-diyl)] |
| PBTI3T | poly[*N*-(2-hexyldodecyl)-2,2′-bithiophene-3, 3′-dicarboximide-alt-5,5-(2,5-bis(3-decylthiophen-2-yl)-thiophene)] |
| PCE | power conversion efficiency [%] |
| $Pd(PPh_3)_4$ | tetrakis(triphenylphosphine)palladium(0) |
| p-DTS$(FBTTh_2)_2$ | 7,7′-[4,4-Bis(2-ethylhexyl)-4H-silolo[3,2-b:4,5-b′]dithiophene-2,6-diyl]bis[6-fluoro-4-(5′-hexyl-[2,2′-bithiophen]-5-yl)benzo[c][1,2,5]thiadiazole] |
| PEDOT:PSS | poly(3,4-ethylenedioxythiophene) polystyrene sulfonate |

| | |
|---|---|
| PTCDA | perylene-3,4,9,10-tetracarboxylic dianhydride |
| PTB7 | poly({4,8-bis[(2-ethylhexyl)oxy]benzo[1,2-b:4,5-b′]dithiophene-2,6-diyl}{3-fluoro-2-[(2-ethylhexyl)carbonyl]thieno[3,4-b]thiophenediyl}) |
| PTB7-Th | poly([2,6′-4,8-di(5-ethylhexylthienyl)benzo[1,2-b;3,3-b]dithiophene]{3-fluoro-2[(2-ethylhexyl)carbonyl]thieno[3,4-b]thiophenediyl}) |
| PV | photovoltaics |
| Rpm | rotation per minute |
| Rt | room temperature |
| TD-DFT | time dependent density function theory |
| TGA | thermogravimetric analysis |
| TMS | tetramethylsilane |

# Table of Content

# 1 Introduction

Global energy demand grew by 2.3% last year which can be attributed to the high economic growth worldwide. It is caused by the increasing population and its rising need of energy for heating, cooling, transportation etc. If we have a look on the global electricity demand the growth for 2018 reached 4% for which largely the expanding electro mobility can be associated.[1]

As it can be seen in Figure 1, most of the used electricity is produced out of non-renewable sources like coal, natural gas or oil. Nevertheless, these resources are limited, and they also contribute to the rising $CO_2$ levels in the atmosphere and therefore cause global warming. Hydropower with 15.7 % and wind power with 5.5% are the next largest suppliers followed by solar photovoltaic with 2.4%. These values seem to be small, but they have risen steadily over the last years. Together they reached the new high level in the last year, making it possible to cover 26.2 % of the global electricity production. [2]

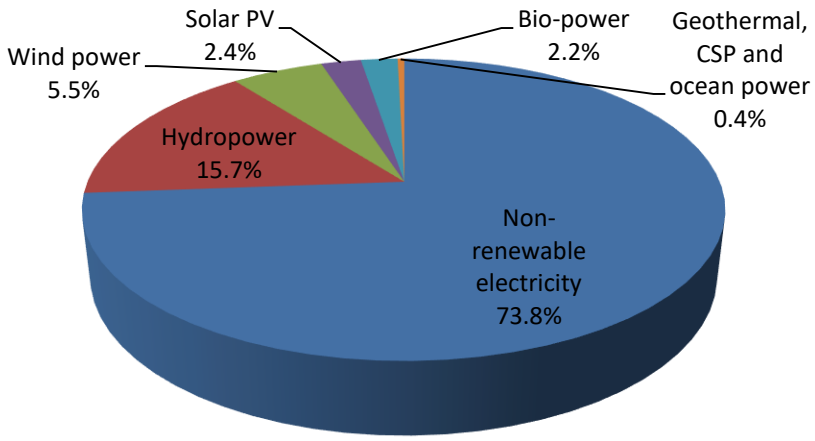


**Figure 1: Estimated Global Electricity Production, End-2018; data used from reference.**[2]

Renewable resources possess a high potential for energy production but still face various challenges. For example, they struggle with low efficiencies for harvesting the so-called free energy around us. Apart from that, the intermittent nature of solar or wind power makes it hard to provide a constant supply of energy. On a sunny day solar photovoltaics might be able to cover the energy demand needed, but on a cloudy winter day it might not produce a single watt. As a result, suitable storage possibilities are unavoidable to cover the energy demand continually every day of the year.[3]

## 1.1 General photovoltaics

Photovoltaics which can produce electricity from sunlight can be divided into three different generations. The first generations consist of single crystal or multi crystal silicon based solar cells. The first silicon solar cell was developed by the Bell Laboratories in 1954 with an efficiency of 6%.[4] These first-generation solar cells were further developed over the years and count to around 80% of all solar panels in use today. The second generation is also called thin-film solar cells because they consist of thinner layers compared to the crystalline silicon based solar cells. They include amorphous silicon, cadmium telluride (CdTe), copper-indium selenide (CIS) and copper-indium-gallium-diselenide (CIGS) solar cells. Although their efficiencies are lower than the first-generation ones, they are quite interesting because of their lower production costs. The third and latest generation focuses on dye sensitised solar cells (DSSC), perovskite based solar cells and organic or also called polymer solar cells (OPV).[5,6]

## 1.2 Organic solar cells

In organic photovoltaics electricity is generated due to the absorption of irradiated light in a organic semiconductor. The photoactive layer in organic photovoltaics consists of a bilayer or a mixture of two organic semiconductors. One is used as electron donor and the other as electron acceptor. There are already a broad range of material combinations reported in literature: for example, small molecules only, polymer only or combinations of polymers and small molecules as donor and acceptor materials. However, one of the most widely studied combination is a polymer, with a conjugated π-system, and a fullerene derivative.[7] Due to their high synthetic costs and lack of tuneability regarding energy levels research nowadays focuses on so called non-fullerene materials.[8,9] In an organic solar cell the acceptor and donor material together represent the active layer between two electrodes. Interfacial layers between the electrodes and the active layer alleviate the charge transport to the electrodes respectively. The hole transport layer (HTL) transports the holes, whilst being transparent to the incoming light. Electrons on the other side are transported by the electron transport layer (ETL) which also protects the active layer from damage during the deposition of the cathode. Furthermore, they both provide a barrier for excitons so they cannot recombine on the interface of the electrodes. As it can be seen in Figure 2, the above described active layer can be structured in two different ways. For instance, the first solar cells possessed a bilayer structure where a layer of the donor material

was covered by a layer of the acceptor material. This setup had the big drawback of limiting the charges which can be generated by the interface area between the two layers.

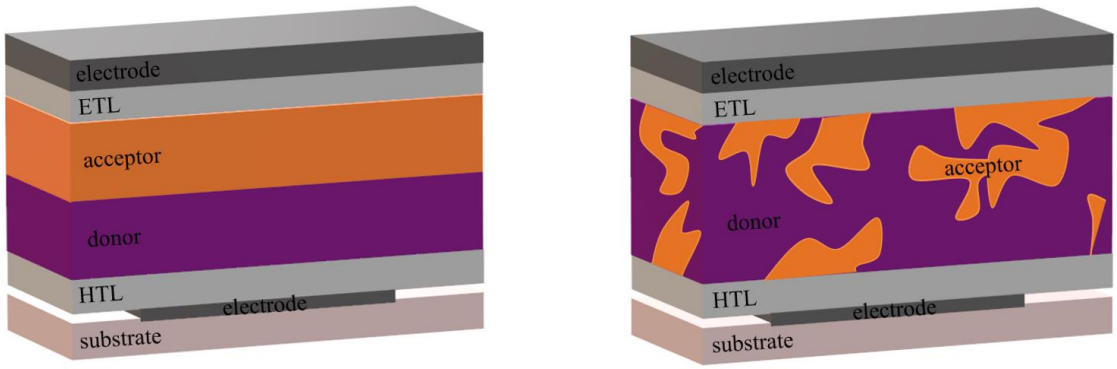


**Figure 2: Comparison of a bilayer-heterojunction (left) and bulk-heterojunction (right) solar cell setup.**

Consequently, a new setup called bulk-heterojunction (BHJ) was developed. Here the two materials are blended together and applied as one layer, thereby increasing the interface area between the materials significantly. However, the bulk-heterojunction setup also faces some challenges. The intermixing of the two materials, the solvent used, the donor acceptor ratio or the thermal annealing are only a few factors that can have a big impact on the active layer and its final morphology. Besides that, there is also the possibility of building out so called island inside the active material. These islands have no contact to the electrode and therefore in it generated charges cannot be separated.[10,11]

The way how the charges in a solar cell are collected can be divided into two different device architectures, (see Figure 3). The normal structure generally consists of a transparent, high work function anode on the glass substrate and a low work function metal cathode on top of the active layer. In the inverted device structure, the positions of the anode and cathode are turned around. Thereby, electrons are collected by a transparent metal oxide ($TiO_2$, ZnO) and the holes by a high work function metal (Ag, Au). The use of the inverted setup is preferred because of its higher stability under ambient atmosphere.[12,13]

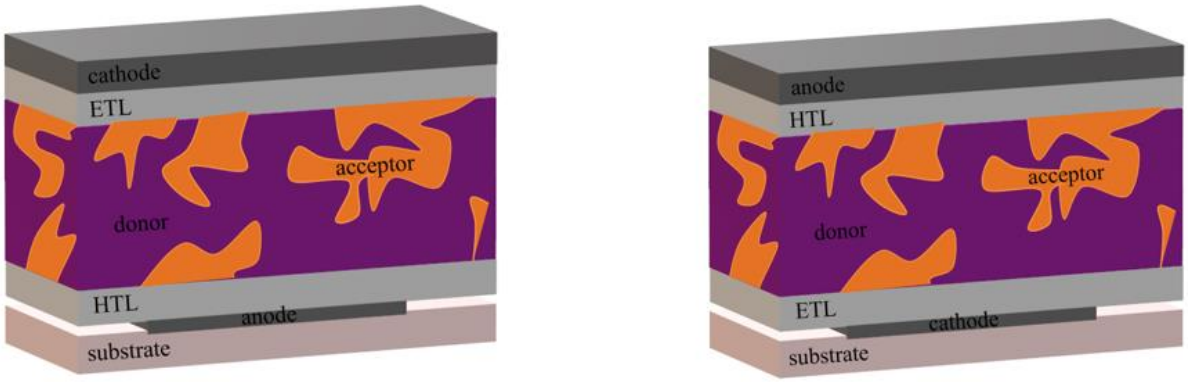


**Figure 3: Bulk-heterojunction solar cell in normal (left) and inverted (right) device architecture.**

Figure 4 shows the charge generation mechanism of an organic solar cell. The absorption of photons generates an electron-hole pair or also called exciton. This exciton produced in the donor material must diffuse to an interface area between the donor and acceptor material within its lifetime otherwise it will decay. The diffusion length is limited by exciton lifetime consequently reducing the usable layer thickness. On the interface the charges of the exciton are separated and can now be transported to the electrodes, respectively.

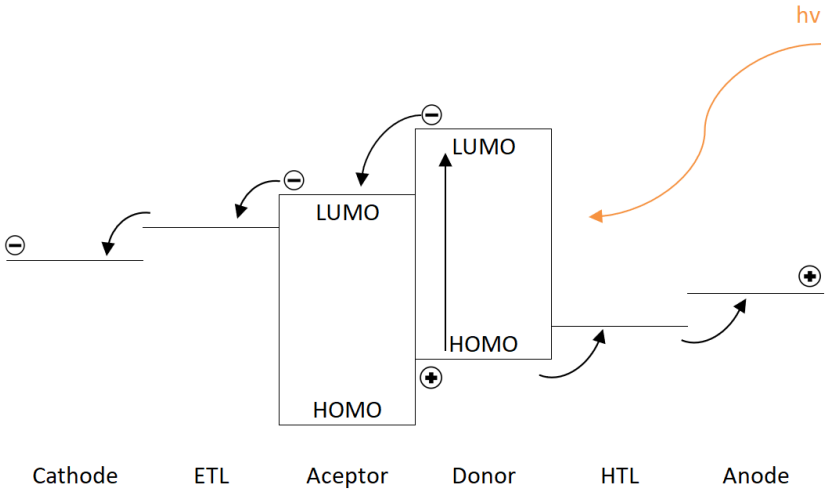


**Figure 4: Generalized charge generation mechanism of an organic solar cell.**

It is necessary to overcome the exciton binding energy for the charges to be separated. Therefore, a driving force is needed which is provided by the energy difference of the donor LUMO and acceptor HOMO material. The exciton binding energy for organic semiconductors lies in range of around 0.3 to 0.5 eV. It is described by Equation 1 where e is the electronic charge, ε the dielectric permittivity of the material, $\varepsilon_0$ the vacuum permittivity and r the distance between the electron and hole.[14]

$$E_B = \frac{e^2}{4\pi\varepsilon\varepsilon_0 r} \quad (1)$$

Equation 1 shows that the exciton binding energy can be reduced by increasing the dielectric permittivity of the material and thereby reducing the needed energy difference between the donor and acceptor material. That could result in an increased $V_{OC}$.

The photons which can be absorbed in an organic solar cell are limited to the bandgap of the materials used. There are also other factors that limit the efficiency. The so-called Shockley-Queisser limit describe the limitations of efficient energy conversion. In general, it says that photons with a lower energy than the given bandgap do not contribute to the energy production, however all photons with a higher energy take part in the process, but their excess energy is lost in a thermalization mechanism. That together limits the overall maximum efficiency to 30% for single junction solar cells with a bandgap of 1.1 eV and non-concentrated illumination.[15,16]

## 1.3 Characterisation of solar cells

Solar cell devices are mainly characterized by their current-voltage curve represented in Figure 5. The curve is obtained by sweeping the voltages on the solar cell while measuring the current under illuminated and dark conditions. The light measurement is performed under standardized conditions at 25 °C and a light intensity of 1000 W/m$^2$. The light used is also called AM 1.5 which simulates the sun spectra with an incident angle of 48.2° shining onto the earth surface.[15,16]

From the measured curve the efficiency to produce electricity by the solar cell can be determined. Therefore, the current is converted to current density [mA/cm$^2$] regarding the solar cell size used. In the curve the current density under short-circuit ($J_{SC}$) conditions can be seen where the curve measured under illumination cuts the y-axis. It is mainly influenced by the absorption of the active material, the charge carrier mobilities and the charge separation efficiency. So, when choosing new materials for organic solar cells, compounds with broad absorption range are favoured.

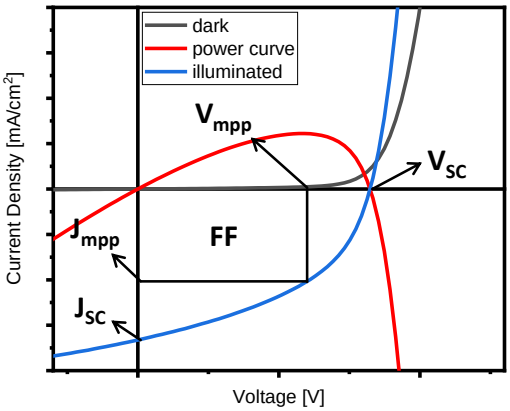


**Figure 5: Main characterisitic parameters of a *J-V* curve.**

The next important parameter is the open circuit voltage ($V_{OC}$). Defined as the voltage at zero current or with other words the maximum voltage the solar cell can produce. It is approximately corresponding to the energy gap between the LUMO of the acceptor and the HOMO of the donor. The measured value for the $V_{OC}$ commonly does not fit to the calculated energy gap because it is affected by radiative and non-radiative loses which can reduce the $V_{OC}$.[9,17,18]

The $J_{mpp}$ and $V_{mpp}$ describe the current density and voltage at the maximum power point. At this point the device produces the most possible power output. The maximum power point can be accessed easily by multiplying the voltage with the measured current at each point and checking the largest value in the power curve. With these parameters other values to describe the solar cell performance can be calculated. Such as the fill factor (FF). According to equation 2 it can be calculated by dividing the product of $J_{mpp}$ and $V_{mpp}$ by the product of $J_{SC}$ and $V_{OC}$.

$$FF = \frac{J_{mpp} * V_{mpp}}{J_{SC} * V_{OC}} \qquad (2)$$

It describes the ratio between the real produced power and the power that could be theoretically possible. Or in other words how "square" the measured J-V curve occurs. In an ideal situation the value for the FF would be 1, but because of factors like shunt resistance and series resistance influencing the FF this value is always below one.[19]

$$PCE = \frac{P_{out}}{P_{in}} = \frac{V_{OC} * J_{SC} * FF}{P_{in}} \qquad (3)$$

The most important parameter of a solar cell is the power conversion efficiency (PCE) calculated by equation 3. It reveals how much of the irradiated light can effectively be converted into electricity. Since the PCE consists of the values discussed before it is also influenced by the same parameters.[20]

## 1.4 State of the art

History of bulk-heterojunction solar cells is way shorter compared to other solar cell systems. It started in 1986 when Tang published the first heterojunction solar cell consisting of a donor acceptor system with nearly 1% efficiency.[21] From that point a lot of different donor acceptor cells were tested containing dyes, polymers, fullerenes, non-fullerenes or small molecules.[22] Up till now the best organic solar cell consists of a polymer and a non-fullerene acceptor. The best solar cell device has a $V_{OC}$ of 0.867 V, a very high $J_{SC}$ of 25.4 mA/cm$^2$ and an FF of 75% resulting in the all-time high efficiency of 16.5%.[23]

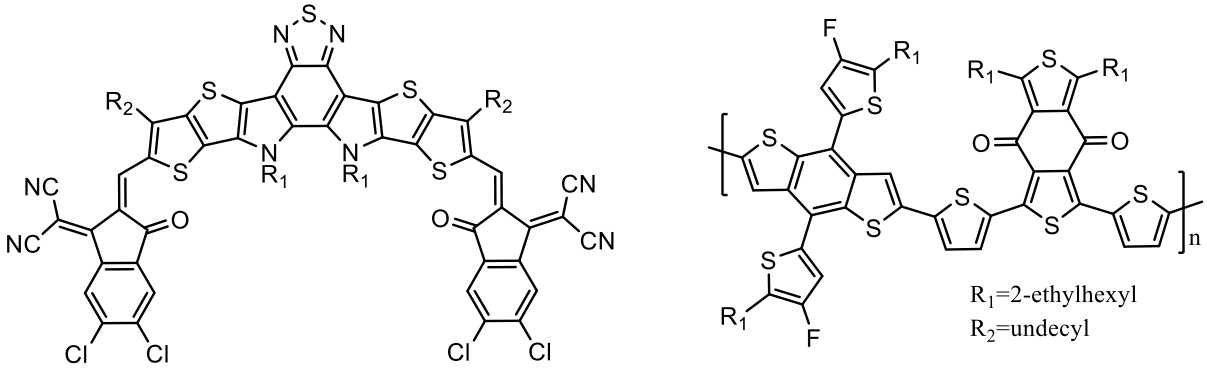


**Figure 6: Structure of the acceptor (left) and donor polymer (right) used in the best organic solar cell.**

In Figure 6 the chemical structures of the used donor (PBDB-TF) and acceptor (BTP-4Cl) material can be seen. It must be mentioned that the structure of the acceptor consists of chlorine and cyano side groups. Also, the polymer contains halogens in its structure. Typical for this type of structure is the conjugated system with an electron rich core flanked by electron poor units forming an acceptor-donor-acceptor (A-D-A) structure. This conjugated push pull structure can be found in many of the latest publications, like the very high efficient ITIC derivatives.[24]

To study the effect of these and other side groups in this thesis, a different structure called perylenediimide was used as an acceptor. Perylenediimdes bear many different advantages compared to other structures used as acceptors in solar cells. Due to their high stability, they are also broadly used as pigments in industry.[25] The starting material is very cheap and can be modified easily by a few synthesis steps. Perylenes offer different possibilities for modification, see Figure 7. New substituents can be introduced into the core structure at ten different sites, divided into ortho, bay and imide position. Perylene derivatives were already used by Tang in his first heterojunction solar cell, but also in dye based photovoltaic cells.[26]

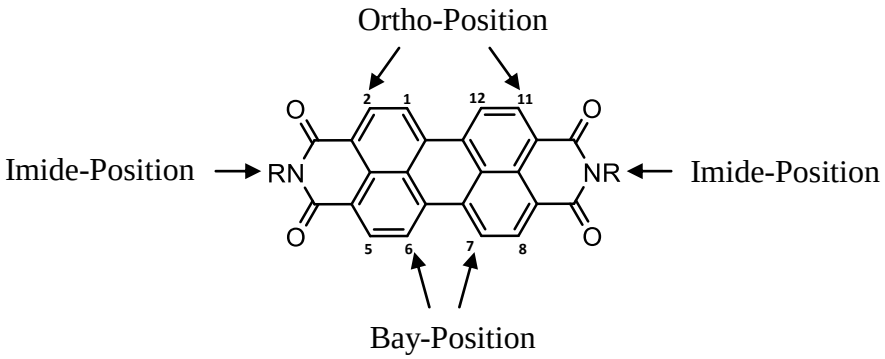


**Figure 7: General structure of a perylene diimide.**

J.P. Sun et al. studied the influence of different branched alkyl side chains at the imide position on the photovoltaic performance of organic solar cells, see Figure 8 **1a-d**. They tested perylenes with four different side chains mixed with F-DTS as small molecule donor in a normal device setup: ITO/PEDOT:PSS/BHJ/PDIN/Ag. The results showed that the 1-ethylpropyl side chain leads to the highest efficiency of 3.21%. Compared to the 1-propylbutyl (PCE=1.98%) or the 1-heptyloctyl (PCE=0.19%) side chain it is a large difference considering that the optical properties of all compounds are nearly indistinguishable. For the compound with the 1-ethylhexyl side chain negligible low efficiencies were obtained. Since the nitrogen atom lies in the nodal plane of the perylene the substituent on the imide position has negligible influence on the optical properties. For that reason, the difference in power conversion efficiencies is mainly caused by improved active layer intermixing and morphology.[27] Y. Chen et al. reached even an efficiency of 5.13% for the same perylene diimde, donor material and device setup by changing the donor acceptor ratio from 1:1 to 1.3:1 D/A. It must be mentioned that in this publication calcium was used as electron transport layer and alumina as electrode.[28] More examples with longer branched-alkyl side chains or unbranched alkyl side chains can be found in literature, see Figure 8 **2a,b**. Nevertheless, none of them exceeds an efficiency higher than 0.5%. In the

case of the branched side chains P3HT was used as donor polymer which practically overlaps with the absorption region of the perylene compound. For that reason, only a small part of the light spectrum could be covered resulting in a low power conversion efficiency than probably possible.[29,30] J. Qu et al. introduced another way of imide position modification by proposing a new design concept consisting of a donor-spacer-acceptor co-oligomer structure, see Figure 8 **3a-c**. With the optimum spacer length of four carbon atoms an efficiency of 2.33% could be reached. Although the efficiency is not the largest, this compound reached a remarkable high $V_{OC}$ of 1.04 V. The co-oligomer was tested in a normal solar cell setup consisting of: ITO/PEDOT:PSS/Co-oligomer/epPDI/LiF/Al.[31] A similar molecular design was published by Y. Lu et al. were a donor-acceptor-donor structure was built by introducing tetraoctyl-bisfluorene groups on both imide positions, see compound **4** in Figure 8. This acceptor was tested with P3HT as donor polymer in a normal device setup: ITO/PEDOT:PSS/BHJ/Al providing 0.13% efficiency without any further solar cell device optimization.[32]

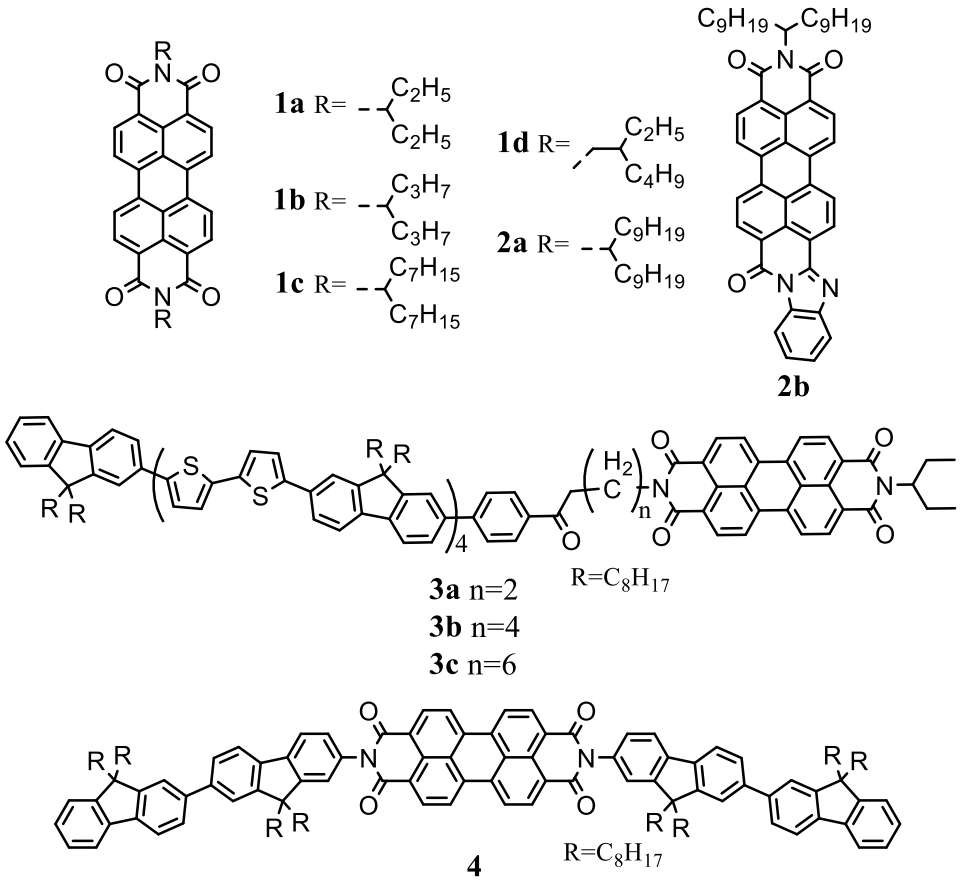


**Figure 8: Perylene diimides with different substituents on the imide position.**

In 2011 V. Kamm et al. first tested an ortho alkylated perylene in organic solar cells, see Figure 9 compound **5**. In combination with P3HT and a normal cell setup of ITO/PEDOT:PSS/BHJ/Al

a doubling of solar cell efficiency could be observed compared to the non-alkylated compound. This was reasoned by the improved solubility and lowered aggregation caused by the alkyl chain in the ortho position. Although the maximum efficiency did not exceed 0.5 %, the impact of core substitution on the efficiency was pointed out.[33] P.E. Hartnett et al. investigated the stacking of different ortho substituted perylene compounds and their influence on the power conversion efficiency. The study suggest that the phenyl substituted perylene (**6a**) achieved a maximal slip-stacking, followed by the phenethyl perylene (**6b**) and the hexyl perylene (**6c**). The slip-stacking quenches the excimer formation while sustaining an efficient π-stacking for charge transport resulting in a power conversion efficiency of 3.67% for the phenyl perylene. Although other acceptors reached lower efficiencies, all of them reached a $V_{OC}$ higher than 1 V. The solar cells were built with PBTI3T as donor polymer in an inverted setup (ITO/ZnO/BHJ/$MoO_3$/Ag).[34]

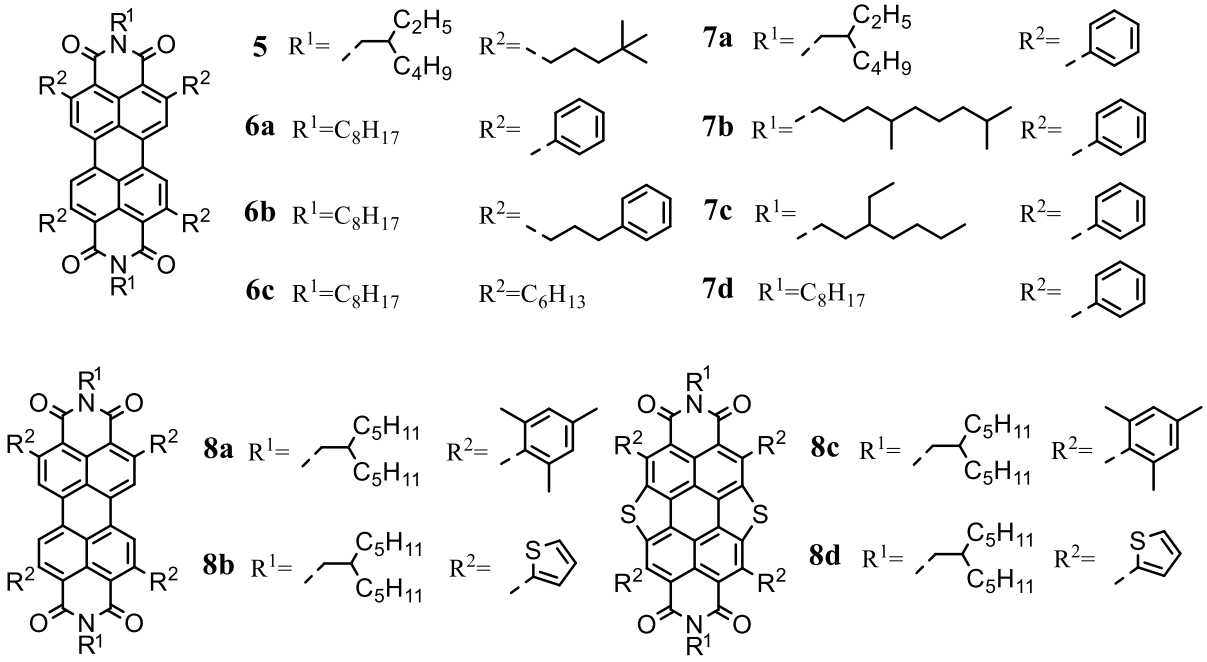


**Figure 9: Examples for ortho (2,5,8 and 11 position) substituted perylene diimides.**

In another work P.E. Hartnett et al. showed that the phenyl perylene can crystalize in two different packing motifs depending on the substituent on the imide position and the crystallization conditions. They found that a sterically hindering substituents like 3-pentyl (**7a**) favours a herringbone packing while n-octyl (**7d**) substituent tend to form a slip-stacked structure. The 3,7-dimethyloctyl substituent (**7b**) could be directed in either of them by varying

the 1,8-diiodooctane (DIO) concentration. The article demonstrated higher efficiencies for the slip-stacked structures. In particular the n-octyl and the 3,7-dimethyloctyl substituent on the imide position reached 3.88% and 3.62%, respectively. The structures were tested with PBDTT-FTTE as polymer donor in an inverted device architecture (ITO/ZnO/BHJ/$MoO_3$/Ag).[35] Li X. et al. reported a new one-step Grignard reaction for the functionalization at the ortho position of perylenes. By introducing a mesitylene (**8a**) or a thiophene (**8b**) substituent into the ortho position a solar cell efficiency of 2.55% and 2.97% could be reached. In addition, the substituents were also tested with the S-annulated perylene structure in the bay region. Resulting in an efficiency of 1.30% for the mesitylene (**8c**) and 5.07% for the thiophene (**8d**) substituted compound. The acceptors were blended with PTB7-Th and tested in inverted device architecture (ITO/ZnO/BHJ/$MoO_3$/Ag).[36]

In 2005 W.S. Shin et al. published a paper about different functional groups in the 1,7-bay position of perylenes and their impact on the photovoltaic performance. The studied solar cell devices showed quite low efficiencies of 0.005% for the cyano substituted and 0.043% for the pyrrolidinyl substituted perylene, see Figure 10 **9a,b**. The perylenes were tested in a normal device setup (ITO/PEDOT:PSS/BHJ/LiF/Al) with P3HT as donor polymer.[30] Sharma G.D. et al built a small molecule organic solar cell with perylene diimide holding two tert-butylphenoxy substituents at the 1,7-bay position (**10a**). Combined with BTD-TNP and no transport layers the normal device setup of ITO/BHJ/Al delivered an efficiency of 2.85 %. The good efficiency was attributed to the high lying LUMO level and the balanced charge carrier mobilities.[37] By changing the substituent on the imide position from an anthracene to an acetonaphthopyrazine dicarbonitrile (**10b**) or a pyrene (**10c**) an efficiency of 3.88% or 3.17% could be reached, respectively. Both materials were tested in normal device architecture.[38,39] Different types of phenyl units in mono-bay position were studied by Yi J. et al. By varying the chain length in para position of the phenyl group no difference in the optical and electrochemical properties could be observed. The tested solar cells demonstrated the highest efficiency of 0.74% for the propyl chain (**11a**), followed by 0.39% for the nonyl (**11c**) and 0.37% for the hexyl chain (**11b**). In this case P3HT has been used as polymer in an inverted device structure (ITO/ZnO/BHJ/$MoO_3$/Al).[40] In another work Yi J. and his group studied the influence of an isopropyl group in para (**10a**), meta (**10b**) and ortho (**10c**) position at the phenyl unit. They came to the result that the isopropyl group in meta position delivers the best efficiency of 1.12% compared to 0.82% for the para and 0.71% for ortho position. The improved efficiency of the meta substituted compound was attributed to its higher electron mobilities and better

morphology. It was also shown that the achievable efficiency could be increased from 1.12% to 1.73% by using PTB7 instead of P3HT as donor polymer. All devices were built in inverted structure (ITO/ZnO/BHJ/$MoO_3$/Al).[41]

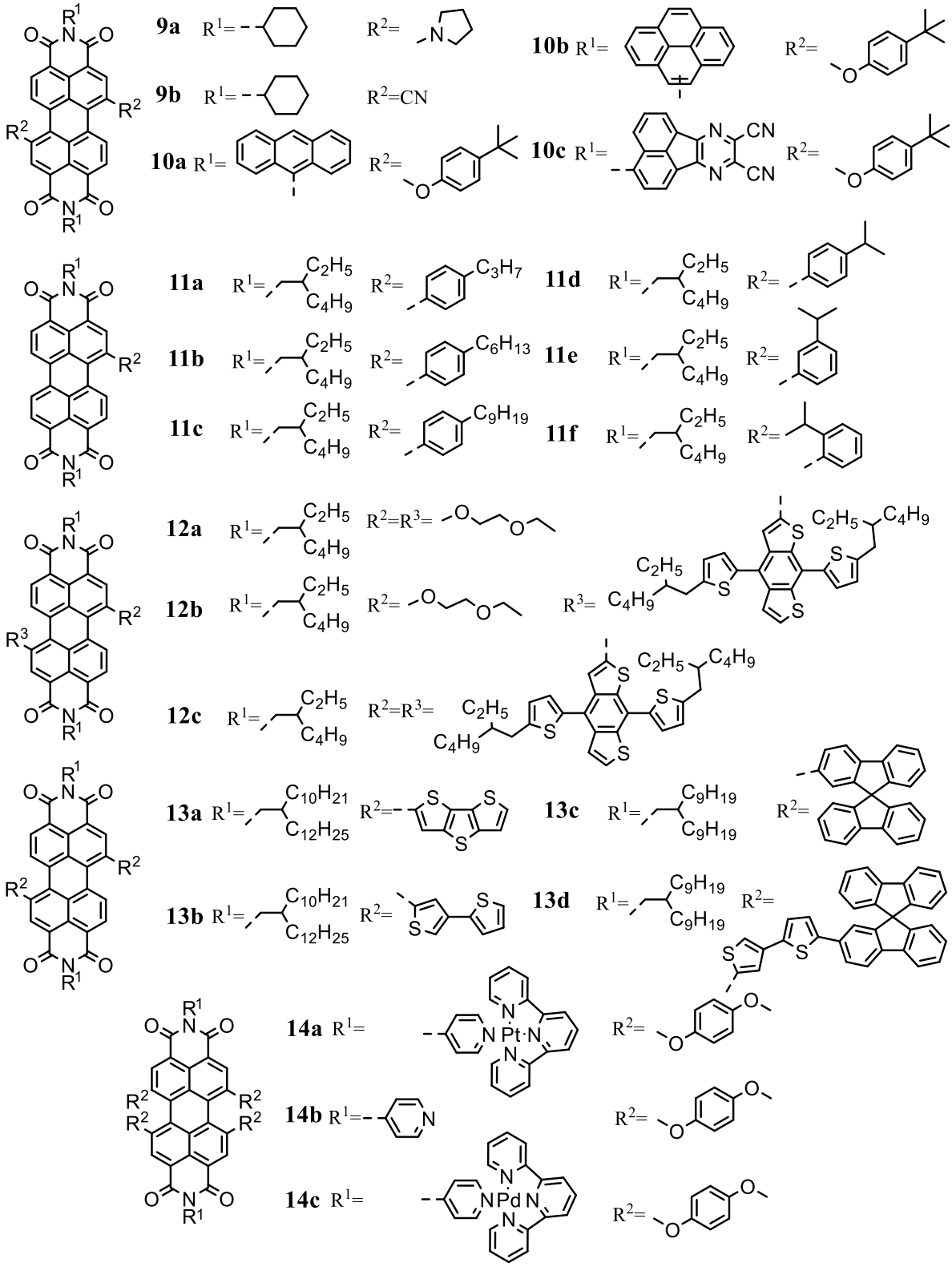


**Figure 10: Various bay (1,6,7 and 12 position) substituted perylene diimides.**

By changing the bay substituent from a 2-mehtoxylethoxyl unit to a 4,8-bis(5-ethylhexylthienyl)-benzo[1,2-b′:4,5-b′]-dithiophene (BDT) unit one by one X. Zhang and his group could cause a red shifted absorption enabling the perylene compound to absorb near infrared light. When tested in organic solar cells an increase in efficiency from 0.005% (**12a**) to 0.44% (**12b**) by exchanging one 2-methoxylethoxyl unit and up to 1.66% (**12c**) by exchanging both 2-methoxylethoxyl units. The improved solar cell performance was caused by the twisted perylene structure due to the BDT substituents and their influence on the absorption range. It created a complementary absorption area when combined with the donor polymer P3HT.[42] P. Cheng et al. studied the influence of different types of donor materials. For their investigation a perylene with dithienothiophene units in the bay position (**13a**) was used as an acceptor. The authors came to the conclusion that a higher mobility and preferable morphology could be obtained when using the small molecule donor p-DTS(FBTTh$_2$)$_2$ compared to the polymer donor PBDTTT-C-T. Resulting in an efficiency of 2.52% for the small molecule donor and 0.28% for the polymer donor when tested in normal device setup (ITO/PEDOT:PSS/BHJ/Ca/Al).[43] In the work of Kotowski D. et al. the influence of bithiophene (**13b**), spirobifluorene (**13c**) and bithiophene spirobifluorene (**13d**) in 1,7-bay position of the perylene were examined. The different perylene compounds were blended with P3HT as polymer donor and tested in a normal device setup (ITO/PEDOT:PSS/BHJ/Ca/Al). The best solar cell efficiency of 1.58% was obtained by the spirobifluorene substituted perylene, caused by its balanced charge carrier transport properties. The bithiophene spirobifluorene and bithiophene exhibited efficiencies of 1.18% and 0.81% respectively.[44] S.I. Büyükeksi et al. published the most efficient mono perylene diimide solar cell device as far as it is known. The used perylene with 4-methoxyphenoxy groups in all four bay positions and a pyridine linked to the imide position (**14b**) achieved an efficiency of 3.91%. By coordination of 2,2′:6′,2″-terpyridyl-platinum (II) (**14a**) or -palladium (II) complex ions (**14c**) on the pyridine, efficiencies of 8.17% and 5.18% could be reached. The perylene compounds were tested in a normal device architecture (ITO/PEDOT:PSS/BHJ/LiF/Al) with P3HT as polymer donor.[45] Beside those, there are a lot more different perylene compounds known by now, which have not been tested in solar cells yet. Like the perylene compounds synthesized by Ma et al. In their work they synthesized a perylene compound with a diethylsilane substituent bridging both bay position of the perylene and the side product where only one side is bridged by the substituent.[46]

A different way of modifying perylenes lies in the building of di-, tri- or tetra perylenes through linking single perylene compounds. This method also offers a variety of possibilities, by linking on different positions and with different linkers. Another option is to build core expanded perylenes usually achieved by UV radiation of bay substituted perylenes. Also, polymeric perylene compounds can be utilized for the application in organic solar cells.[47] Figure 11 shows an example for each of the categories. It has to be mentioned that those perylenes deliver a bit higher efficiency than the mono perylene diimides. Here the depicted polymeric perylene (**15d**) achieves an efficiency of 7.57 % when tested with PTB7-Th in inverted device architecture (ITO/ZnO/BHJ/$V_2O_5$/Al). The authors point out that it possesses a remarkable stability against oxygen and water in the air. While building devices under ambient air with 90% humidity and no encapsulation a decrease in efficiency of only 1% was observed.[48] The tetra perylene [**15c**] linked by a BDT-TH unit and the tri perylene [**15b**] linked by an 1,3,5-triazine were both tested with PTB7-Th as donor polymer and in inverted device architecture (ITO/ZnO/BHJ/$MoO_3$/Ag). They achieved power conversion efficiencies of 8.47 % and 9.15% respectively.[49,50]

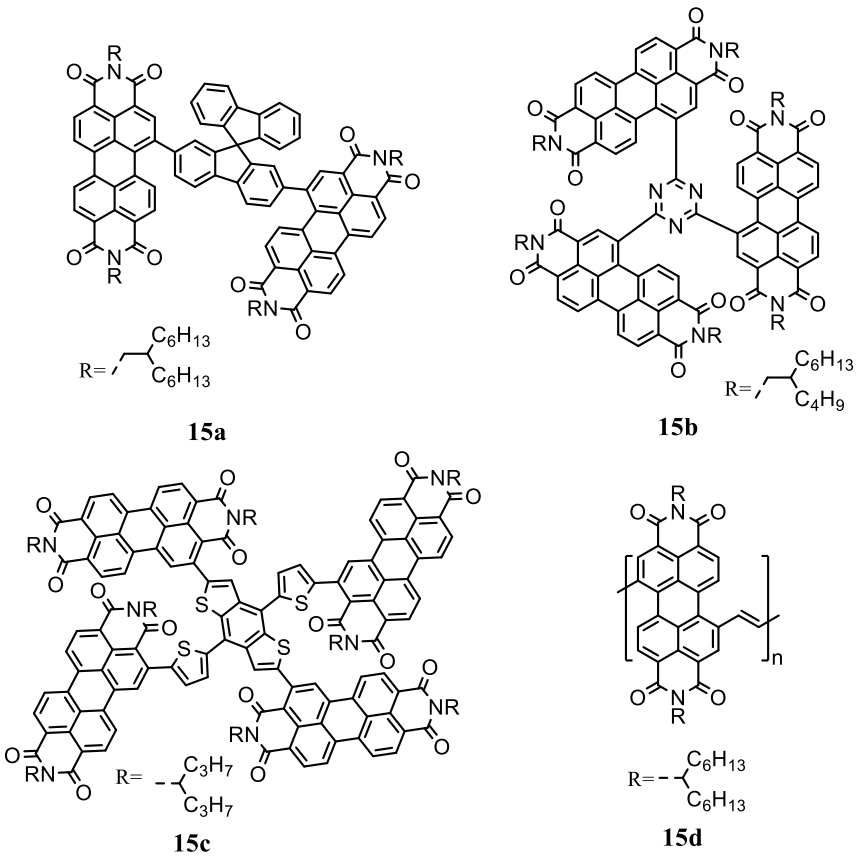


**Figure 11: Examples for di-, tri-, tetra- and polymeric- perylene compounds.**

The highest here discussed efficiency was obtained by the di perylene [**15a**] compound linked via a spirobifluorene unit. When tested with P3TEA as polymer donor the devices achieved an

efficiency of 9.5% with a very high $V_{OC}$ of 1.11 V. On one hand the good performance of this compound was attributed to its fast and efficient charge separation and on the other hand, on its low energy gap between the LUMO of the acceptor and the HOMO of the donor which reduced the voltage losses and enabled a high $V_{OC}$.[51]

## 1.5 Aim of the thesis

This thesis focuses on the synthesis of non-fullerene acceptors for organic solar cells. Recent studies suggest that materials with a higher dielectric permittivity (ε) used in organic solar cells can lead to enhanced solar cell efficiencies. According to literature there are different ways of increasing the dielectric permittivity. For example, by introducing different substituents into the structure like e.g.: ethylene glycol chains, cyano groups or halogens like fluor.[52] A chemical compound with a structure that can be modified easily should be used. The structure should be modified by different substituents and their influence on the optical properties, energy levels and solar cell performance should be studied. Additionally to the experimental data the synthesized compounds should also be evaluated by density functional theory calculations. For that reason, the geometry should be calculated and specifications like the absorption maximum, oscillator strength and dipole moment predicted. After the synthesis their optical and electrical properties are characterized and their usability as non-fullerene acceptors tested with matching donor materials. Furthermore, the built organic solar cells should also be characterized, and their performance further improved. Therefore, different building parameters are varied, like the active layer thickness, the annealing behaviour or the donor and acceptor ratio. A correlation between calculated values and the experimental data of the solar cells should be found to give promising suggestions for further material designs.

# 2 Results and Discussion

## 2.1 Synthesis

Starting from PTCDA (perylene-3,4,9,10-tetracarboxylic dianhydride) novel acceptors with different substituents in the bay region were synthesized (Figure 12). To study the impact of the different bay substituents, the imide position was left the same for every compound. 2,6-diisopropylphenyl was chosen as substituent for the imide position because of its steric demanding character it increased the solubility in comparison to the starting material very well. It was seen that the bay substituents not only changed the optical and electronic properties but had also an additional impact on the solubility of the compound by twisting the perylene structure.

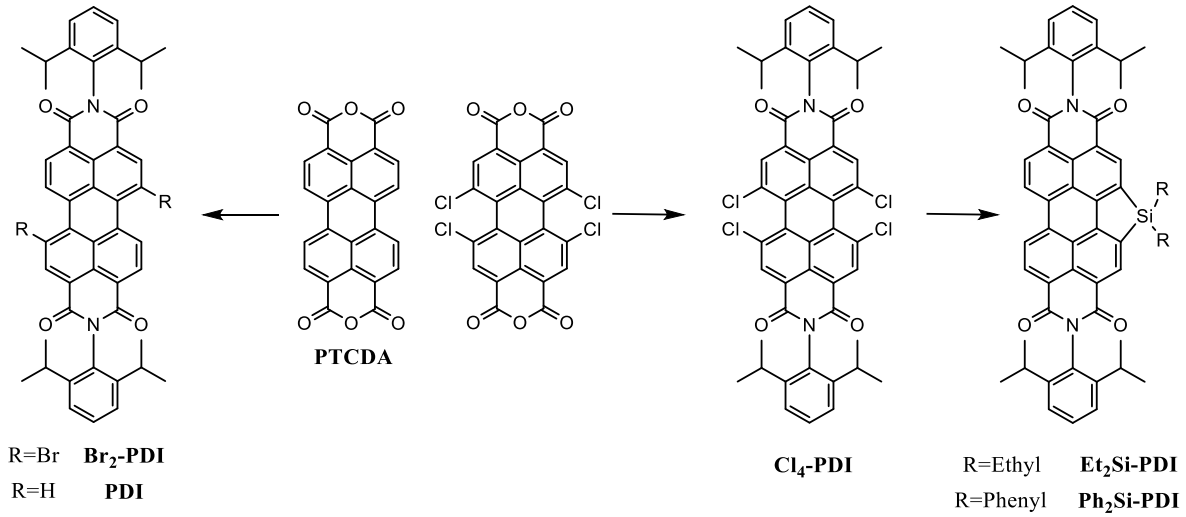


**Figure 12: Overview of the different synthesized perylene derivatives.**

### 2.1.1 PDI

The reaction of PTCDA with 2,6-diisopropylaniline (4 eq) and with imidazole as base leaded to the pure perylene compound (PDI) see (Figure 13).[53] The reaction mixture was stirred under $N_2$ atmosphere at 180 °C. Compared to first approaches the high reaction time of 44 hours mainly increased the yield up to 66 % resulting in a brown-red solid. The measured $^1$H NMR spectrum is in agreement with literature and is shown in the appendix, Figure 31. After column

chromatography with DCM as eluent the product was further purified by recrystallization from DCM and methanol. The product possessed a much better solubility than the starting material. Nevertheless, the solubility was still rather poor compared to the bay substituted compounds. This can be explained by π-π stacking of the perylene central core.[54]

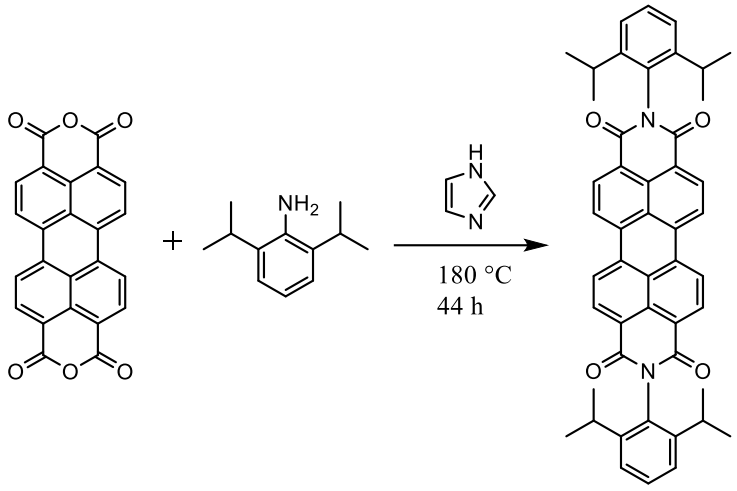


**Figure 13: Reaction scheme for the synthesis of PDI.**

The optical spectrum of PDI is discussed in comparison to the other compounds in chapter 2.1.6. Thermogravimetric (TGA) measurement shows a loss in mass starting at 478 °C demonstrating the high stability of the perylene diimide, see Figure 30 in the appendix.

## 2.1.2 $Br_2$-PDI

For the introduction of bromine in the bay position PTCDA was suspended in concentrated sulfuric acid, see Figure 14. After the addition of small amounts of iodine, 6 equivalents of bromine were slowly added with a syringe leading to the formation of 2. Due to the lack of solubility, the crude product was used in the next step directly after the work up. In the second step 2 was suspended in propionic acid and let to react with 4 equivalents of 2,6-diisopropylaniline. After column chromatography an isomeric mixture of 1,7 and 1,6 dibromo perylene bisimide was isolated.

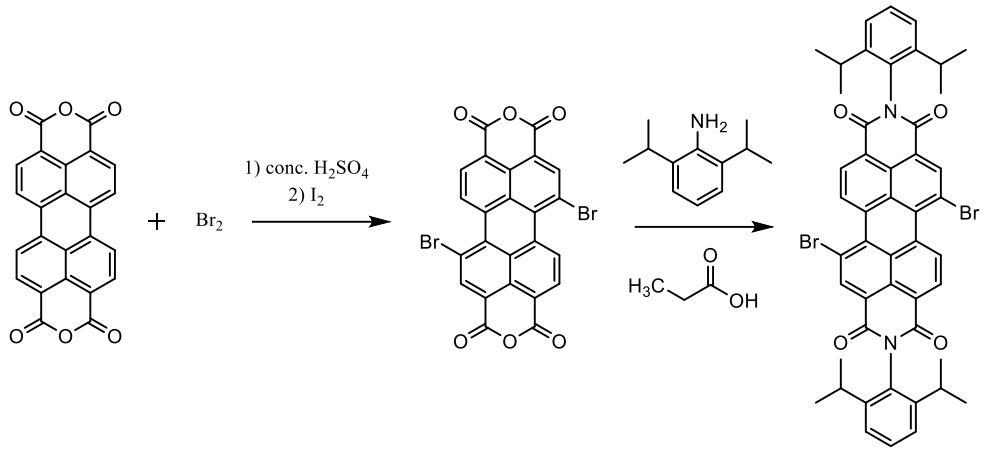


**Figure 14: Reaction scheme for the synthesis of $Br_2$-PDI.**

Würthner *et al.* discussed the problem of the 1,7 and 1,6 regioisomers in his publication.[55] They suggested to separate the two regioisomers by recrystallization. Therefore, the product was dissolved in dichloromethane and covered by a layer of methanol. The so grown crystals were than isolated. This process was repeated six times. Due to the narrow differences in the chemical shifts the two isomers could be only observed in a high filed $^1$H NMR spectrum. In a low field spectrum, the signals just overlap. Figure 15 shows the $^1$H NMR spectra of the recrystallization process. Eventually an orange-red solid could be isolated. The entire spectrum is shown in the appendix, Figure 32 and is in agreement with literature.[55]

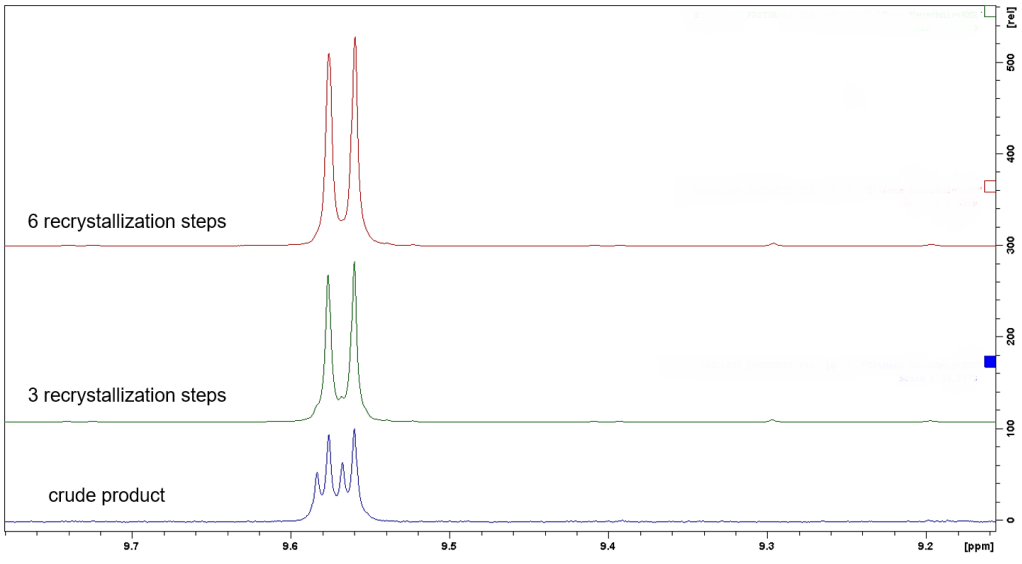


**Figure 15: $^1$H NMR spectroscopic observation of the recrystallization process; 500 MHz $^1$H NMR spectra.**

Nevertheless, regarding solubility the bromine substituent has an impact. During synthesis $Br_2$-PDI appeared to be better soluble than the PDI compound. That could be a result of the bromine forcing the perylene into a twisted structure in which it is hindered to do a π-π stacking. The

TGA curve, depicted in Figure 30 in the appendix, shows a mass loss at 393 °C resulting in a lower stability compared to the PDI compound.

### 2.1.3 $Cl_4$-PDI

For the last two perylene compounds $Cl_4$-PTCDA (tetrachloro-perylene-3,4,9,10-tetracarboxylic dianhydride) was used as starting material. Firstly, it was suspended in propionic acid and let to react with 2,6-diisopropylaniline, (Figure 16). After column chromatography an orange solid was obtained in high yield. The TGA displays a thermal stability up to 443 °C for $Cl_4$-PDI.

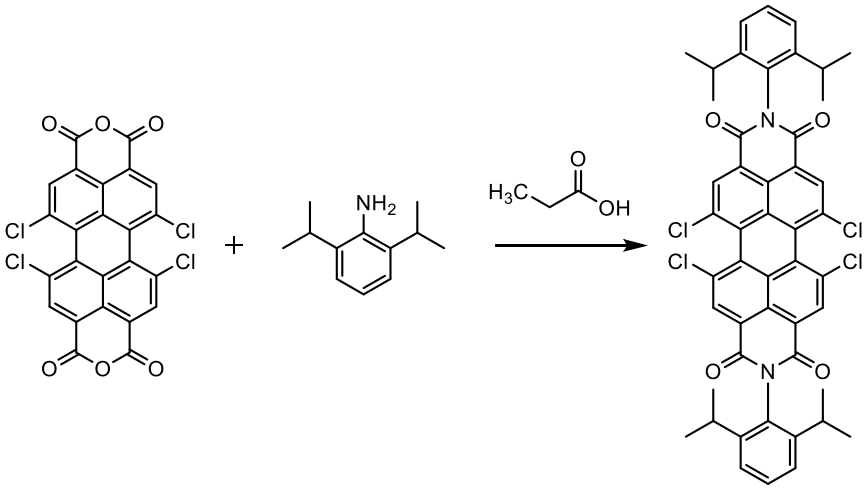


**Figure 16: Reaction scheme for the synthesis of $Cl_4$-PDI.**

The solubility is equal to the one of the $Br_2$-PDI compound based on the twisted perylene structure.

### 2.1.4 $Et_2Si$-PDI and $Ph_2Si$-PDI

Finally, a silicon was introduced bridging the bay position of the perylene. Therefore the approach of Ma *et al.* was used. In their publication they synthesized a perylene with a diethylsilane bridging both bay positions as main product and mono bridged perylene as side product, by using a palladium-diacetate precursor and tricyclohexylphosphine to catalyse the reaction.[46] In this work two different silanes were used for the reaction, once a diehtylsilane and once a diphenylsilane. Therefore, the prior synthesized product $Cl_4$-PDI was used as starting material. $Cl_4$-PDI was dissolved with potassium acetate and 7 equivalents of diethylsilane or diphenylsilane in dry toluene. A palladium (0) ($Pd(PPh_3)_{4)}$ was used as catalyst, see Figure 17. Unfortunately, the substitution on all bay position, as it was described in the

paper, could not be achieved for either one of the silanes. After column chromatography a red solid could be obtained as product for both silanes. During the reaction with the diphenylsilane more side products were produced. Therefore, a second column chromatography with a different eluent was needed resulting in a lower yield. For future reactions the second eluent should be tried first to maybe save one column chromatography.

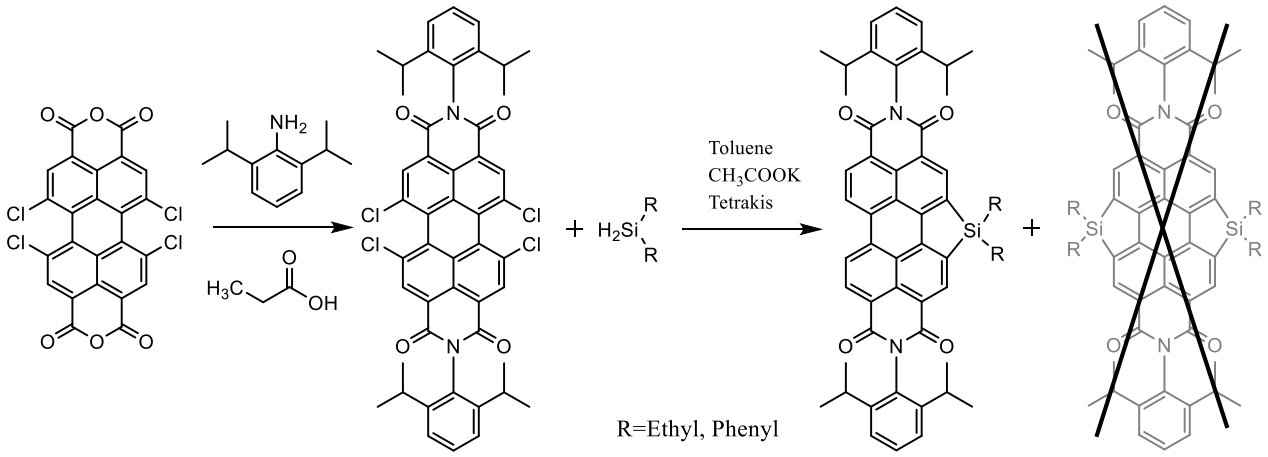


**Figure 17: Reaction scheme for the synthesis of $Et_2$Si-PDI and $Ph_2$Si-PDI.**

Although the silicon does not cause a twist in the perylene structure, the compound retains a similar solubility like $Br_2$-PDI or $Cl_4$-PDI. The ethyl and phenyl side groups can be accounted for the improved solubility, sterically hindering the perylene stacking. TGA measurement of compound $Et_2$Si-PDI shows a loss in mass beginning at 448 °C see Figure 30 in the appendix.

## 2.1.5 Di(O-2-ethylhexyl)-violanthrone

The di(O-2-ethylhexyl)-violanthrone (vio) compound was obtained by an alkylation reaction of violanthrone, see Figure 18. Therefore, the starting material was dissolved with potassium carbonate in DMF. After adding 3 equivalents of 2-ethylhexylbromine, the reaction mixture was stirred for 22 hours at 100 °C. Subsequently the product was worked up and purified by column chromatography resulting in a dark-purple powder. The recorded $^1$H-NMR spectrum is in agreement with literature and is shown in the appendix, Figure 36.[56]

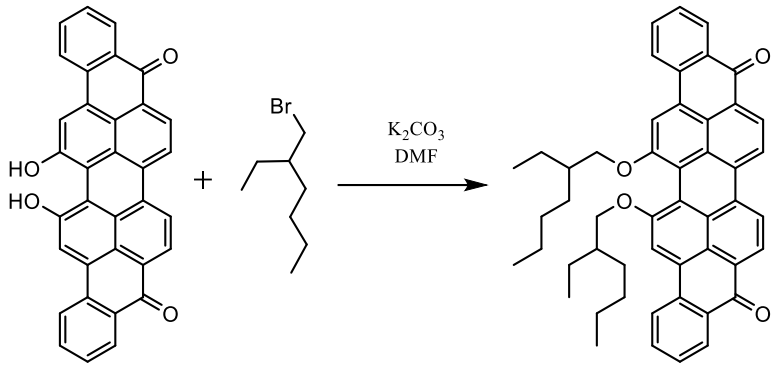


**Figure 18: Reaction scheme for the synthesis of vio.**

According to the TGA measurement the vio compound showed constant mass till 320 °C resulting in a much lower stability compared to the perylene diimide compounds, see Figure 30 in the appendix.

## 2.1.6 Optical spectra

The absorption spectra of PDI showed three peaks with increasing intensity at 455 nm, 490 nm and 527 nm. The corresponding emission spectra showed three peaks at 534 nm, 575 nm and 626 nm with decreasing intensity when exited at 485 nm. The Stockes shift was with 6 nm rather small. From the measured spectra also the quantum yield was calculated to be 99%. That was expected because perylene diimides are known for their high quantum yields.[57] All spectra were recorded in chloroform and are depicted in Figure 19.

The absorption spectrum of $Br_2$-PDI showed the typical perylene pattern with three peaks. Compared to the PDI spectra the peak position showed hardly any difference. However, the first two peaks at 455 nm and 490 nm occur to be broader than the ones of PDI. It seems like the bromine substituent has a rather small influence on the absorption properties. But a stronger one on the emission spectra when exited at 485 nm. The emission spectra show peaks at 548 nm and 585 nm with decreasing intensity. Therefore, the Stockes shift with 20 nm is also higher than the one of the PDI. The quantum yield was calculated to be 94% for this compound.

The $Cl_4$-PDI compound shows also the typical perylene absorption spectrum with a slight shift to shorter wavelengths. In the absorption spectra the peaks appear at 427, 488 and 521 nm with increasing intensity. The higher impact on the optical properties compared to $Br_2$-PDI can probably be attributed to the higher twisted perylene structure of $Cl_4$-PDI. The emission spectra

exited at 485 nm, shows peaks at 550 nm and 585 nm with decreasing intensity. Resulting in a stokes shift of 29 nm. The fluorescence quantum yield was with 89% the lowest for the perylene diimide compounds. The lower quantum yield for chlorinated perylene diimides was also observed by G. Seybold et al.[57]

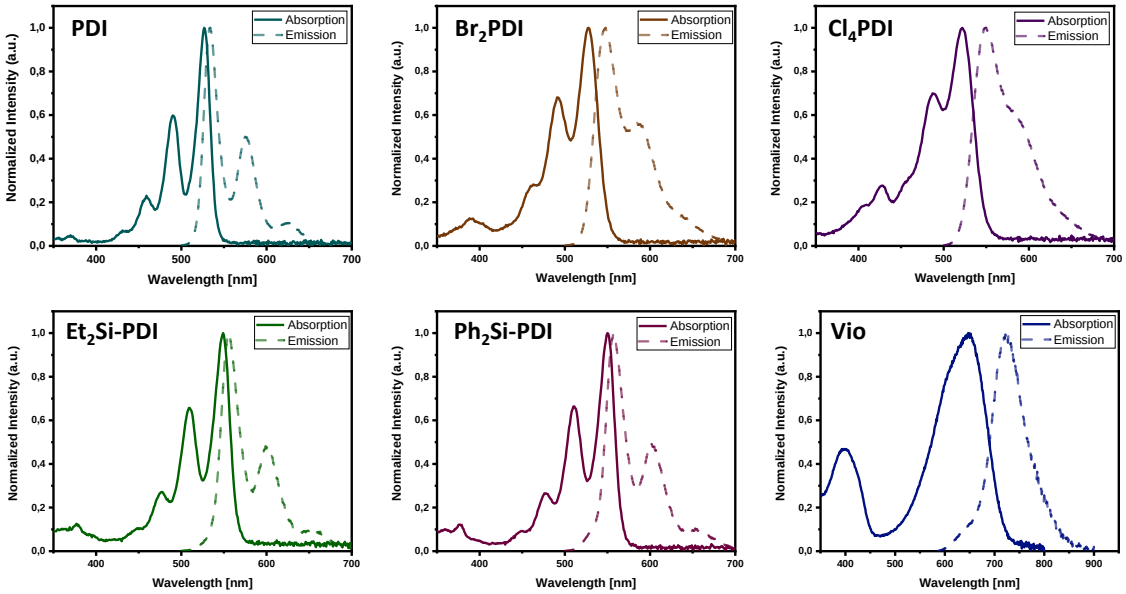


**Figure 19: Absorption and the corresponding emission spectra measured in $CHCl_3$.**

In the absorption spectrum of the last two perylene compounds, again the typical perylene pattern appears. The silicon substituent causes a shift to higher wavelength. The peaks appear at 477, 509 and 548 nm for $Et_2Si$-PDI and 476, 511 and 550 nm for $Ph_2Si$-PDI with increasing intensity. For the emission spectra compound $Et_2Si$-PDI was exited at 492 nm and showed peaks at 555, 599 and 653 nm with decreasing intensity. Compound $Ph_2Si$-PDI was exited at the same wavelength resulting in an emission spectrum of 557, 602 and 653 nm with decreasing intensity. The Stokes shift for both compounds is 7 nm. The fluorescence quantum yield for $Et_2Si$-PDI was 99% and with that the highest of all perylene diimides. $Ph_2Si$-PDI reached a quantum yield of 96%.

The absorption spectra of vio shows a peak at 394 nm and 646 nm with increasing intensity. The compound was excited at 492 nm and had an emission peak at 725 nm. Resulting in a very high Stokes shift of 79 nm. The calculated quantum yield for the violanthron derivative was with 17% much smaller than the one of for the perylene diimides.

## 2.2 Density Function Theory (DFT)

Firstly, the geometry of the perylene compounds was studied. Therefore, the structure was first optimized by ChemDraw3D. The pre optimized structure was used to calculate the optimized molecular geometry using density functional theory. A B3LYP functional with 6-31G* as basis set was used and was calculated with Gaussian 09 (Revision D.01).[68] After the geometry optimization a frequency calculation was conducted to check if the obtained geometry lies in the absolute minimum. In Figure 20 the calculated geometries are depicted. It can be seen that the diisopropylphenyl substituent on the imide position is turned by 90° to the perylene core. Giving the first improvement regarding solubility by hindering the π-π stacking sterically.

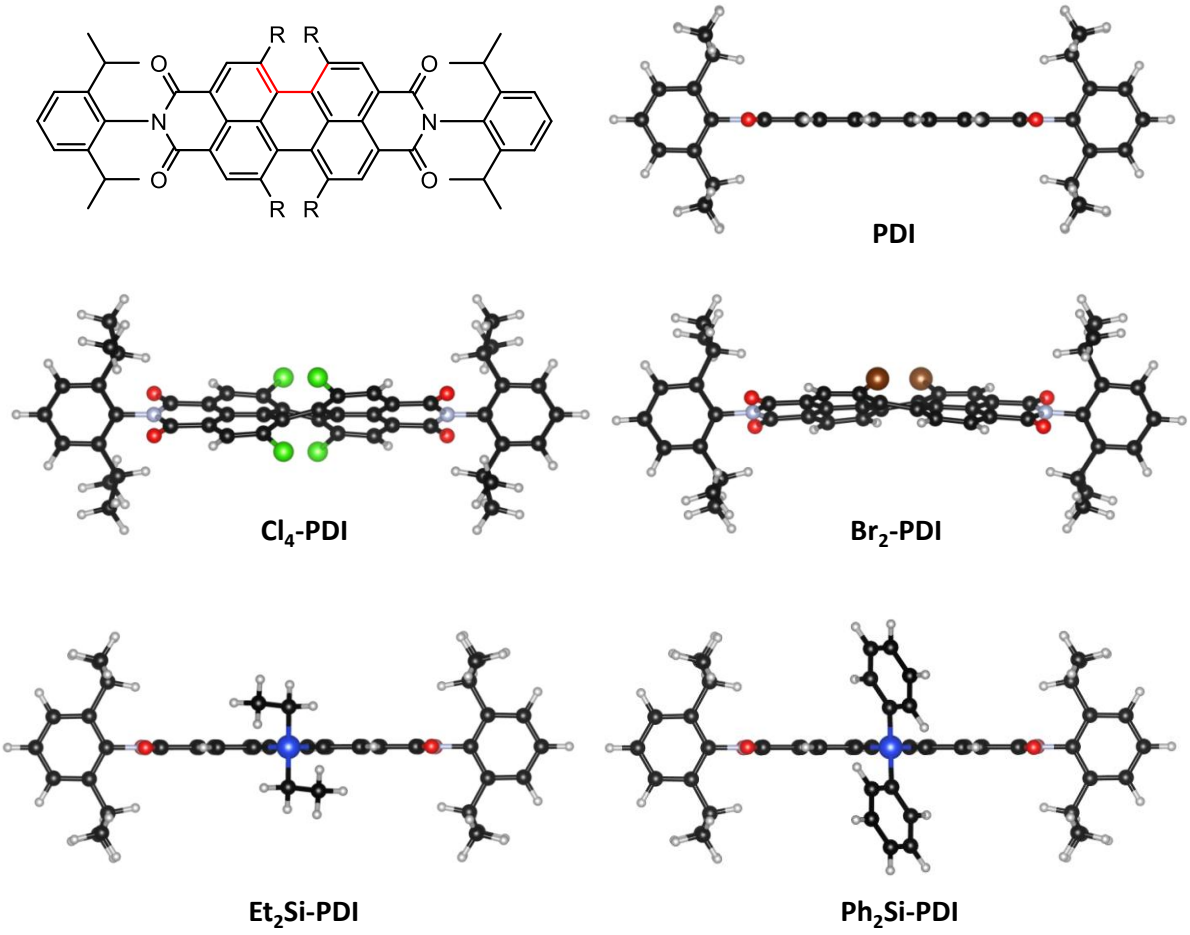


**Figure 20: Optimized geometry of the perylene compounds and the calculated dihedral angle marked in red.**

Furthermore, the dihedral angle marked red in Figure 20 was determined for each substance, representing the twist in the perylene caused by the different substituents. As illustrated compounds PDI, $Et_2Si$-PDI and $Ph_2Si$-PDI show no twist in the perylene structure having a

dihedral angle of 0°. Nevertheless, the ethyl and phenyl side groups on the silicon block the π-π stacking as well. $Cl_4$-PDI has the larger twist of 36° compared to $Br_2$-PDI with 22°. This is due to the higher repulsion of the two chlorine atoms on each side of the perylene compared to the $Br_2$-PDI compound whereas there is only one bromine on each side.

From the optimized geometry also the energy levels of the molecules were obtained. In Figure 21 each substrate is depicted with its HOMO-LUMO level, bandgap and its molecular orbital distribution. In the middle of each acceptor a node is formed from one imide position to the other one with no observable density. That implies that the substituent on the imide position has no influence low the energy level of the molecule. On the substituents of the silicon in $Et_2$Si-PDI and $Ph_2$Si-PDI the same phenomena can be observed suggesting that these substituents have no impact on the HOMO-LUMO shape either. This is verified by the low difference in the energy levels and also in the practically identical absorption and emission spectra of these two compounds.

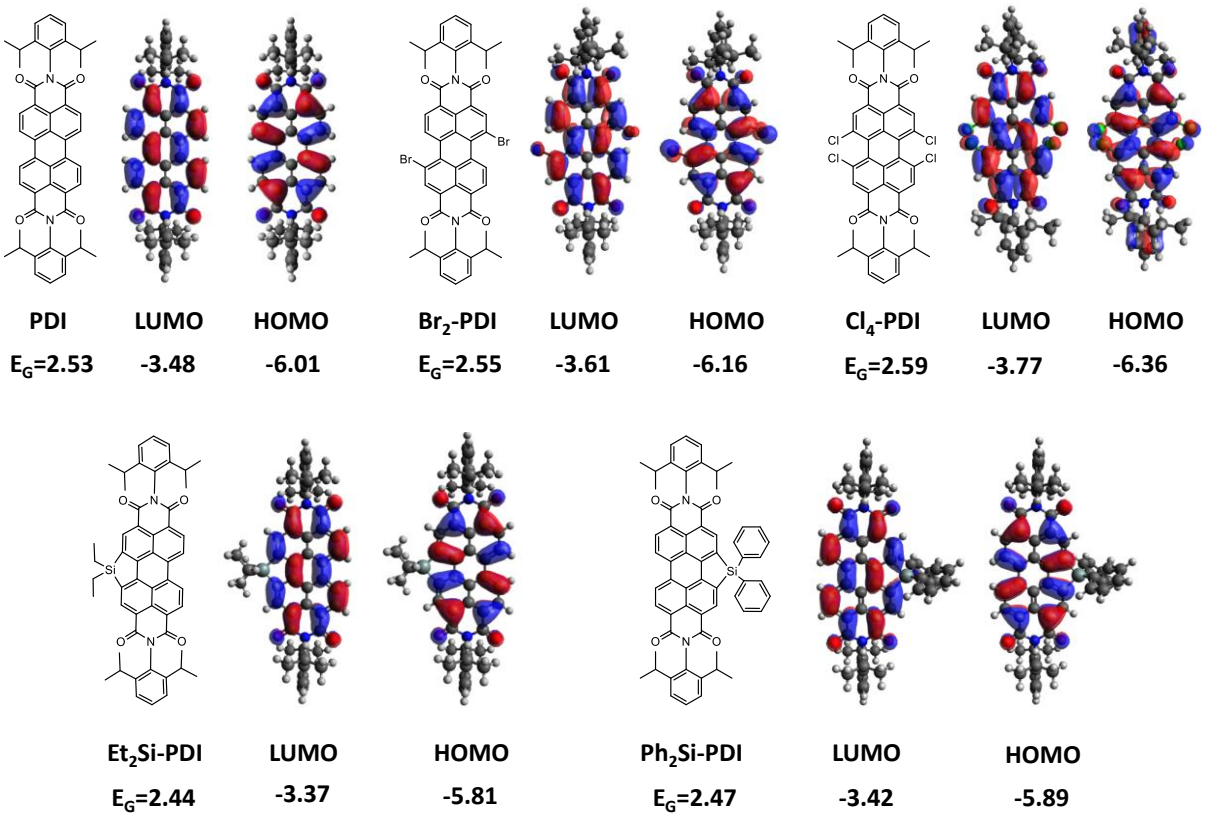


**Figure 21: Bandgap of each perylene compound with the corresponding energy levels and the visualised electron distribution.**

In general, the orbital distribution over the molecules is not changed significantly by the different substituents. In some cases it is just extended to the added substituents. All acceptors

show a large bandgap of around 2.5 eV with rather small variation among each other. What do change indeed are the energy levels. By introducing the bromine atoms into the bay position of the perylene, the LUMO level is shifted from –3.48 to –3.61eV and the HOMO level from –6.01 to –6.16 eV. Considering $Cl_4$-PDI this shift is even higher for the LUMO from –3.48 to –3.77 eV and for the HOMO from –6.01 to –6.36 eV. All that can be explained by the –I effect of the halogens which increases by increasing electron negativity. In contrast, the two silicon substituted compounds $Et_2$Si-PDI and $Ph_2$Si-PDI display slight shifts to higher energy levels.

In the next step the optimized structures were used to calculate the UV-Vis spectra of all compounds by Time Dependent DFT (TD-DFT). Therefore the 6-31+G* basis set with the B3LYP function was used. The calculations were performed in the gas phase. As we see in Table 1 the calculated values are close to the experimental ones, differing in just 11 nm in maximum. Revealing that the used calculation method is suitable to predict the absorption spectra of the perylene compound with different side groups. The calculated oscillator strength on the other hand shows a slight mismatch when compared with the experimentally determined absorption coefficient.

**Table 1: Comparison between the calculated and experimentally obtained data.**

| Substance | $\lambda_{max}^{opt.}$[nm] | $\lambda_{max}^{DFT.}$[nm] | $\varepsilon^{opt.}$ [$M^{-1}$ $cm^{-1}$] | $f^{DFT}$ | Dipole Moment$^{DFT}$ [Debye] |
|---|---|---|---|---|---|
| **PDI** | 527 | 531 | 80400 | 0.69 | 0.00 |
| **$Br_2$-PDI** | 528 | 531 | 43900 | 0.52 | 0.45 |
| **$Cl_4$-PDI** | 521 | 532 | 46900 | 0.47 | 0.00 |
| **$Et_2$Si-PDI** | 548 | 548 | 59500 | 0.68 | 1.15 |
| **$Ph_2$Si-PDI** | 550 | 554 | 39000 | 0.63 | 1.53 |

Considering the symmetry of the perylene compound, it is not surprising that the dipole moment of the first three perylene compounds (PDI, $Br_2$-PDI and $Cl_4$-PDI) is comparable. The silicon substituted compounds on the other hand are not symmetric and therefore also show a higher dipole moment as shown in Table 1.

Additionally, to the synthesized compounds further perylene diimides with various substituents (I, F, Br, Cl, SCN, CN, MeO) in the bay position were calculated with DFT in order to estimate the influence of other substituents on the molecular structure and the optical properties. The obtained data is summarized in Table 2. It must be mentioned here that compound $I_2$-PDI was calculated with a different basis set (3-21G) compared to the others. As it can be seen the different halogens have a rather low impact on the energy levels, the bandgap or the dipole moment. The difference among themselves is minimal. The same is true for the absorption maximum expect for the difluoro compound. Here a shift of 23 nm to shorter wavelengths can be observed compared to the pure perylene diimide compound. Whereas the cyano and thiocyano have a relatively low impact on the absorption maximum. However, because of their strong electron withdrawing character they have a high shift to lower energy levels. In contrast to it stands the methoxy substituted perylene diimide causing an increase in the energy levels with its electron pushing character. It also shifts the absorption maximum by 35 nm to higher wavelengths. The most interesting change in this series is the high dipole moment for the cyano, thiocyano and methoxy group. The thiocyano substituted perylene compound reaches a high dipole moment of 3.15 Debye. Perhaps the reason for that is the thiocyano group itself. Another possible explanation could be the higher length of the substituent. This enables the side group to stand out of the symmetric perylene core and avoids the opposing dipoles to cancel each other out.

**Table 2: Calculated parameters for further bay substituted perylene compounds.**

| Substance | $HOMO^{DFT}[eV]$ | $LUMO^{DFT}[eV]$ | $E_G^{DFT}$ [eV] | $\lambda_{max}^{DFT}$ $[nm]$ | Dipole Moment$^{DFT}$ [Debye] |
|---|---|---|---|---|---|
| **PDI** | −6.01 | −3.48 | 2.53 | 531 | 0.00 |
| **$F_2$-PDI** | −6.08 | −3.52 | 2.56 | 508 | 0.09 |
| **$Cl_2$-PDI** | −6.19 | −3.62 | 2.57 | 535 | 0.62 |
| **$Br_2$-PDI** | −6.16 | −3.61 | 2.55 | 541 | 0.45 |
| **$I_2$-PDI** | −6.24 | −3.69 | 2.55 | 532 | 0.19 |
| **$(CN)_2$-PDI** | −6.52 | −4.06 | 2.46 | 535 | 1.75 |
| **$(SCN)_2$-PDI** | −6.46 | −3.96 | 2.50 | 540 | 3.15 |
| **$(MeO)_2$-PDI** | −5.52 | −3.17 | 2.35 | 566 | 0.97 |

## 2.3 Solar cells

Prior synthesized compounds were tested as acceptors in organic solar cells. For that indium thin oxide (ITO) coated glass substrate as transparent electrode were used. Before activating by plasma etching, the substrates were precleaned with acetone and isopropanol bath. On them a zinc oxide solution as electron transport layer was spin coated. The acceptor was blended with a suitable polymer, with a 1:1 ratio, to give a bulk heterojunction (BHJ). The active layer solution was then spin coated with various speeds to give the optimal layer thickness. It was covered by a molybdenum oxide ($MoO_3$) layer for enhanced hole transport and completed with a silver layer on top to give an inverted solar cell setup. $MoO_3$ and Ag were deposited by thermal deposition under high vacuum.

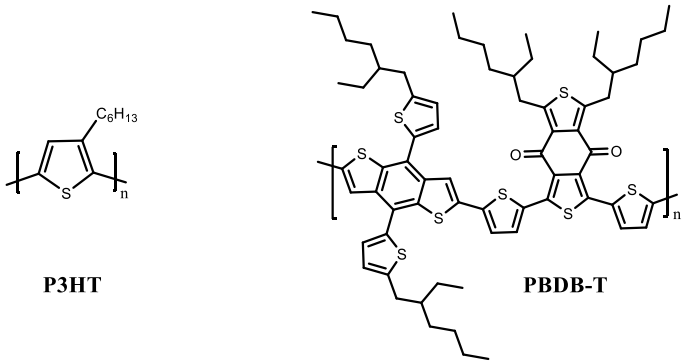


**Figure 22: Used polymers for organic solar cells.**

The polymer was chosen according to its energy levels, complementary absorption spectra and possible miscibility with the acceptor material. For the violanthrone (vio) compound the commonly used P3HT polymer was selected. Due to their similar energy levels, PBDB-T or also called PCE-12 was used for all perylene compounds. The used polymers are depicted in Figure 22. The energy levels of PCE-12 are given by the supplier as -5.33 eV for the HOMO and -2.92 eV for the LUMO.[58]

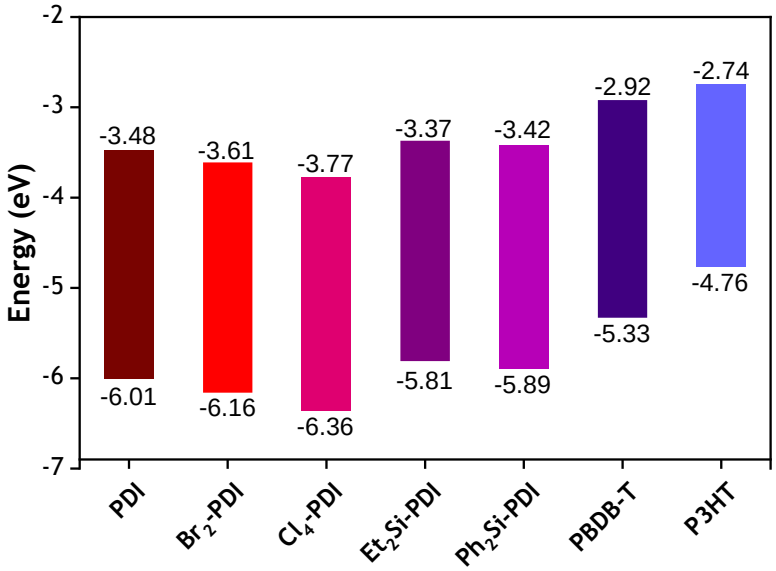


**Figure 23: Energy levels of the acceptors and the polymer donors.**[58,59]

Keeping in mind the path of the charge carriers depicted in Figure 4, these energy levels in combination with the calculated values of the perylene compounds enable efficient charge transport, as it can be seen in Figure 23. Both polymers showed good miscibility properties. Next the absorption range of the donor acceptor blends were investigated. Therefore, the two compounds were spin coated on glass substrate and measured via UV-Vis spectroscopy. As expected, both polymers showed complementary absorption behaviour when combined with the acceptors. This enabled the solar cells to cover a broad range of the solar spectrum. The perylene-poylmer blends absorb in a spectral range from 450 to 650 nm while the violanthrone-polymer blend covers a spectrum from 380 to 680 nm, respectively. The individual absorption areas of each acceptor donor blend are depicted in Figure 24. The vio compound shows an absorption peak at 452 nm which exhibits a blue shift of 30 nm when blended with the polymer P3HT. All perylene compounds exhibit the same typical absorption pattern of a perylene. Although they look very similar, they differ from each other considering the absorption maximum. The silicon compounds $Et_2Si$-PDI and $Ph_2Si$-PDI exhibit the largest shift in absorption maxima to longer wavelength namely 548 and 550 nm, respectively. Compared to the absorption maximum of the pure perylene with 527 nm, this represents a red shift of 21 and 23 nm. While the $Br_2$-PDI and $Cl_4$-PDI compounds show an absorption maximum of 528 and 521 nm, respectively. The higher shift of the chlorine compound related to PDI can be attributed to the higher electron negativity of the chlorine. When measured in films the absorption maxima of all perylene compounds show a slight red shift of around 1-6 nm.

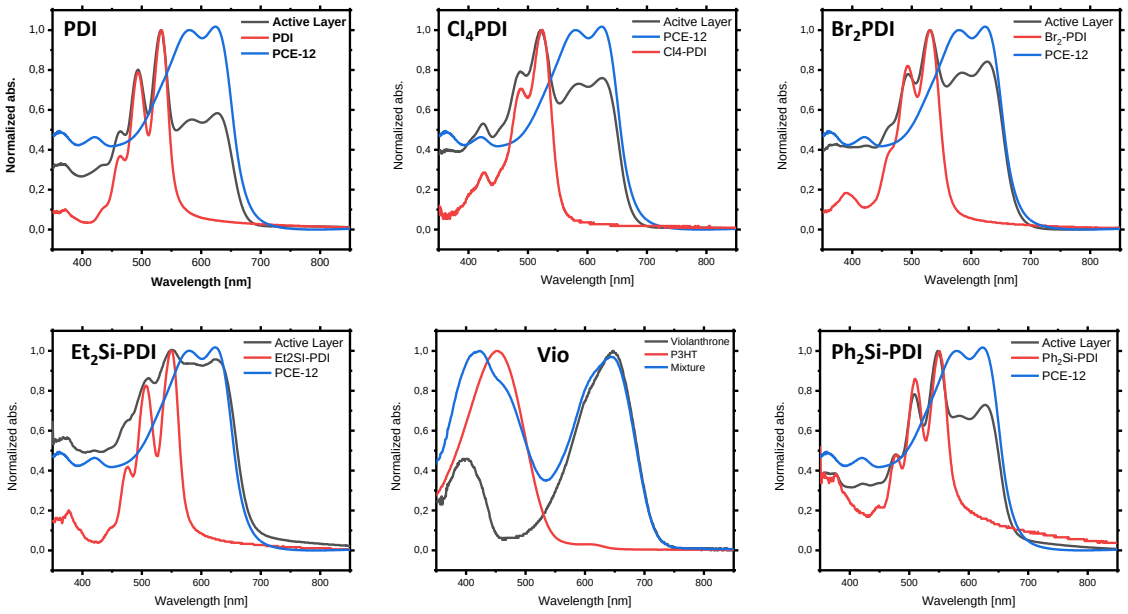


**Figure 24: Normalized absorption of each acceptor, polymer and blend measured in film.**

## 2.3.1 Layer Thickness optimization

The optimum layer thickness of the active layer is a crucial for efficient solar cell devices. Lower values of around 60-160 nm are often found in literature to be optimal.[60,61] Nevertheless, each donor acceptor blend demands its own specific layer thickness due to its difference in charge carrier transport properties. Varying the blend concentration and the spin coating speed offer good ways to change the layer thickness as wanted. For the vio compound the starting concentration of the acceptor was 15 mg/mL and was blended in a ratio of 1:1 with the donor. Although the tested devices exhibited an $V_{OC}$ of 0.67 V the overall power conversion efficiencies were not higher than 0.01%. This did not change by varying the spin coating speed. The layer thickness measurement revealed very thick (200-300nm) and rough layers. For that reason, another series with an acceptor concentration of 12 mg/mL was tested, but with the same result. While the $V_{OC}$ increased to 0.720 V the $J_{SC}$ stayed below -0.4 mA/cm$^2$ resulting again in a very low efficiency of 0.087% in maximum. The layer thickness was again very high. This was attributed the low solubility of the vio compound. For that reason this compound was not further tested in organic solar cells.

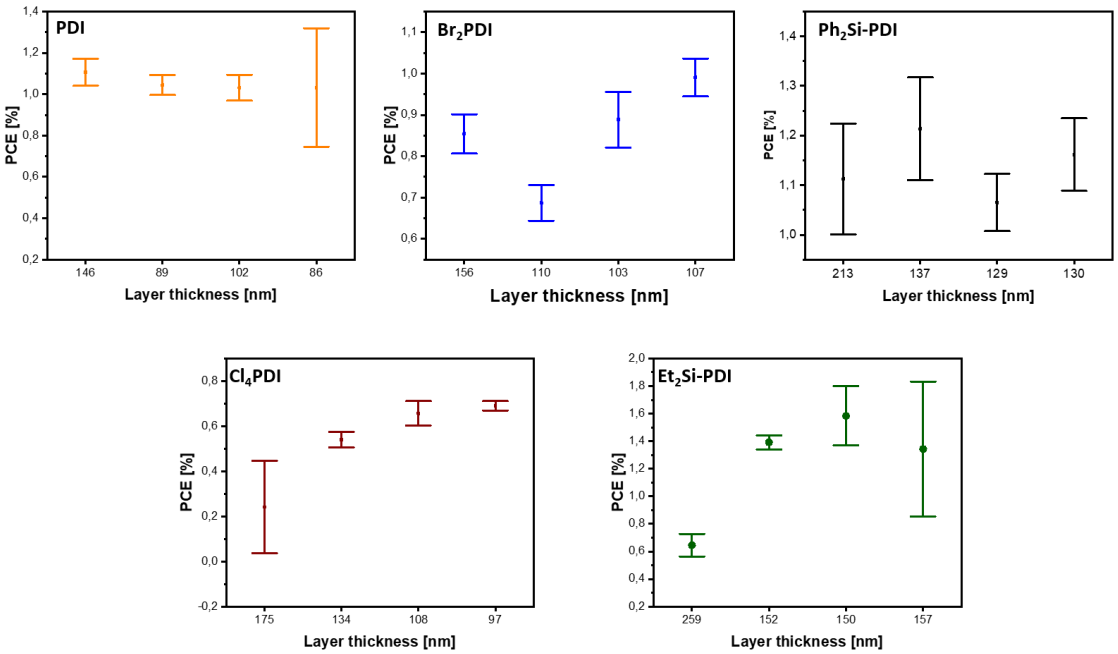


**Figure 25: Spin coating speeds for the processing of the donor-acceptor blends.**

All perylene compounds were first tested with an acceptor concentration of 13 mg/mL, except compound PDI which was tested with 12 mg/mL due to its lower solubility. Figure 25 shows the power conversion efficiency distribution on different spin coating speeds. It can be seen how the efficiency increases with increasing speed and thus lower film thickness. Except compound PDI which displays quite similar efficiencies over a broad range. A constant power conversion efficiency over a broad thickness range makes the commercial production of such solar cell devices easier. When changing the film thickness the $J_{SC}$ and FF of each solar cell primary changes while the $V_{OC}$ stays almost unchanged. Due to its good efficiency over a broad range compound PDI was also tested with a higher concentration of 15 mg/mL resulting in an increased solar cell performance. Since upon a point higher spin coating speed does not influence the layer thickness anymore, the concentration has to be changed to achieve thinner layers. Therfore, the concentration of $Et_2$Si-PDI was changed to 12 mg/mL. By that the layer thickness did not decrease, but the efficiency of the device did increase. In Table 3 a summary of the best parameters and the resulting layer thickness of each acceptor are given

**Table 3: Spin coating parameters and resulting layer thickness of the best performing solar cells of the first series.**

| Acceptor | rpm | layer thickness [nm] | conc. [mg/mL] |
|---|---|---|---|
| **PDI** | 2500 | 241 | 15 |
| **$Br_2$-PDI** | 4000 | 107 | 13 |
| **$Cl_4$-PDI** | 4000 | 97 | 13 |
| **$Et_2Si$-PDI** | 3500 | 147 | 12 |
| **$Ph_2Si$-PDI** | 1500 | 164 | 13 |

## 2.3.2 Light soaking

When building solar cell devices in an inverted structure with metal oxides like ZnO as electron transport layer a so called "light soaking" effect can be observed. This effect describes the improvement of solar cell efficiency under solar radiation over time.[62] One explanation for the increase is the that the trap states are filled up during illumination which cause a reduction of the potential barrier between the ITO and ZnO layer.[63] That can also be seen in the tested solar devices as shown exemplarily for the $Cl_4$-PDI compound in Figure 26. The graphic shows that $J_{SC}$, PCE and FF increase by time, while the $V_{OC}$ stays constant. The impact of light soaking effect on the performance of the solar cells varies among the devices. For that reason, all here represented solar cell data are after an illumination time of 7 min and 20 sec, to guarantee the same light soaking time for each device.

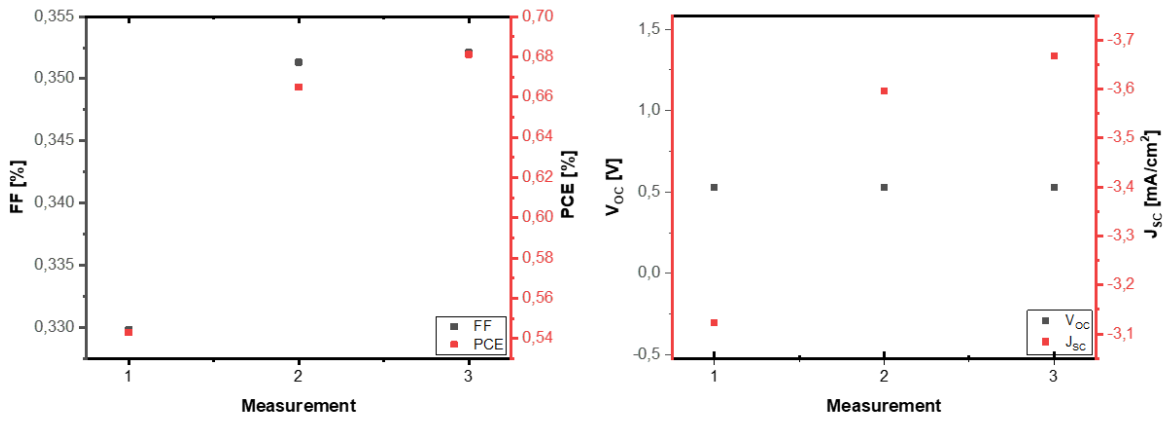


**Figure 26: Effect of the light soaking showed on compound $Cl_4$-PDI.**

### 2.3.3 Annealing Behaviour

Annealing of a solar cell describes a thermal treatment at a certain temperature and over a specific time. There are different ways how the annealing can improve the solar cell performance. On one side it can improve the morphology and intermixing of the active layer when the annealing is done before thermal evaporation. Different types of annealing like the classic one on the heating plate or the so called "solvent vapor annealing" are known.[64] On the other hand, annealing after thermal evaporation has an impact on the interface layer between the active layer and the applied electrodes to improve the charge transfer process. Compound PDI was annealed after thermal evaporation but without an increase in efficiency, probably the used temperatures (80-110 °C) were too low. Due to the high temperature stability of the perylenes also high temperatures can be used for annealing. By annealing the substrate of $Br_2$-PDI at different temperatures the efficiency could be increased. The best increase was obtained at 170 °C for 5 minutes before thermal evaporation to 1.06% compared to the not annealed device which delivered an efficiency of 0.87%. On compound $Cl_4$-PDI solvent annealing, before thermal evaporation, with different temperatures was tested. The efficiency steadily increased by increasing temperature resulting in the highest efficiency of 0.7% when annealed at 120 °C. The annealing behaviour of $Cl_4$-PDI is depicted in Figure 27. It clearly can be seen how the $J_{SC}$ and FF are increased by increasing temperature resulting in a higher efficiency. It has also to be mention that in the same time the $V_{OC}$ experience a slight decrease. The same effect was observed on the other perylene compounds and is also known in literature.[65]

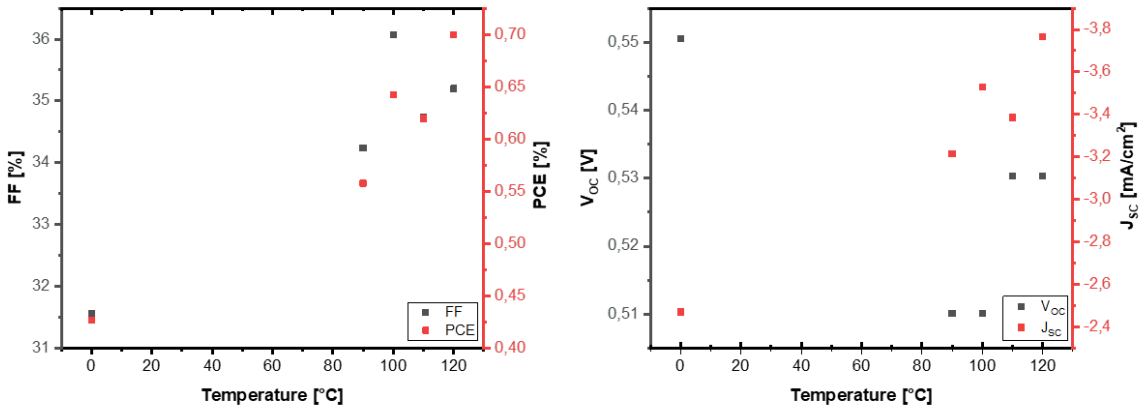


**Figure 27: Effect of the annealing with different temperatures showed on compound $Cl_4$-PDI.**

$Et_2Si$-PDI was also solvent annealed before thermal evaporation at 220 °C resulting in the highest efficiency of 2.42% compared to the 2.11% of the not annealed device.

## 2.3.4 Best solar cells

Finally, the J-V curves (illuminated and not illuminated) and the external quantum efficiencies (EQE) of the best working cells are plotted in Figure 28. It can already be seen in the J-V curves that the $Et_2Si$-PDI acceptor has probably the best solar cells performance, because it has not only a high $V_{OC}$ but also the highest $J_{SC}$.

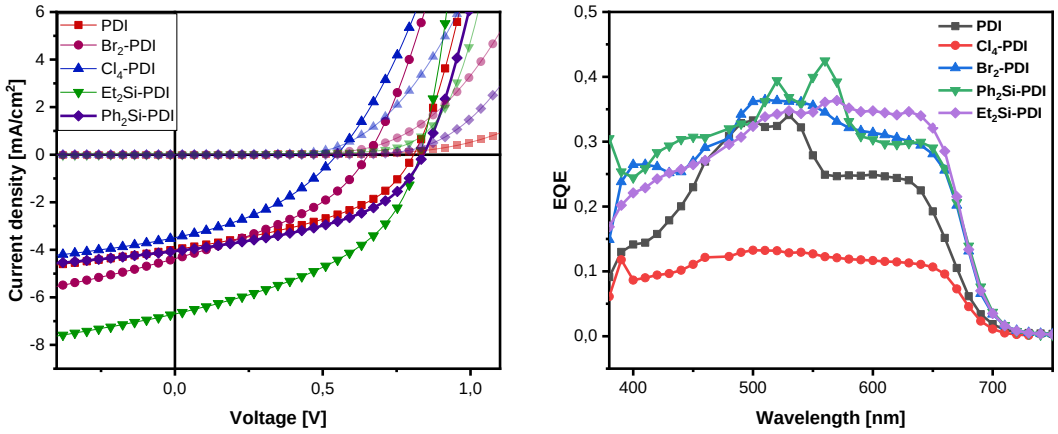


**Figure 28: J-V curves of the best solar cells (left) and EQE curves of each acceptor (right).**

Table 4 gives a summary of the solar cell parameters for each acceptor. Because of their similar energy levels $Et_2Si$-PDI and $Ph_2Si$-PDI have a very comparable $V_{OC}$ of 0.85 and 0.83 V in maximum, respectively. The pure perylene PDI exhibits also a quite high $V_{OC}$ of 0.81 V while the $V_{OC}$ decreases to 0.69 or 0.55 V when bromine or chlorine is introduced into the perylene structure. The bad $V_{OC}$ for the bromine and chlorine substituted compounds can be explained by the lower lying energy levels. As it was shown in Figure 23 the lower LUMO levels decrease the difference between the HOMO of the donor and the LUMO of the acceptor and therefore reduces the possible voltage that can be obtained.

**Table 4: Solar cell parameters of the best solar cell devices.**

| Acceptor | $V_{OC}$ [V] | $J_{SC}$ [mA/cm²] | FF [%] | PCE [%] |
|---|---|---|---|---|
| **PDI** | 0.81 | -3.98 | 42.9 | 1.38 |
| **$Br_2$-PDI** | 0.65 | -4.36 | 37.6 | 1.06 |
| **$Cl_4$-PDI** | 0.55 | -3.48 | 37.3 | 0.71 |
| **$Et_2Si$-PDI** | 0.81 | -6.64 | 45.3 | 2.42 |
| **$Ph_2Si$-PDI** | 0.83 | -4.05 | 46.3 | 1.55 |

The two silicon compounds $Et_2Si$-PDI and $Ph_2Si$-PDI delivered the highest efficiencies, followed by compound PDI, $Br_2$-PDI and $Cl_4$-PDI. It can be clearly seen that the higher efficiency came primarily from an increase of the $J_{SC}$ and the fill factor.

The same picture can be seen in the EQE measurement, in Figure 28. While the chlorine acceptor exhibits external quantum efficiencies of around 10%, the others are around 35%. The highest efficiency of over 40% is achieved by $Ph_2Si$-PDI. One could imagine that compound $Et_2Si$-PDI and $Ph_2Si$-PDI would deliver similar results concerning power conversion efficiency. But this is not the case, although their optical and energetical properties are nearly indistinguishable. The main reason for that probably is the difference in the intermixing caused by the different substituents on the silicon compound. This issue could already be seen during the spin coating of the active layer. While compound $Ph_2Si$-PDI exhibits nice and smooth layers, the layers of compound $Et_2Si$-PDI seemed to contain many particles. This acicular and crystalline structures on the surface seem to be beneficial for the solar cells performance. The light microscope image in Figure 29 shows the difference clearly.

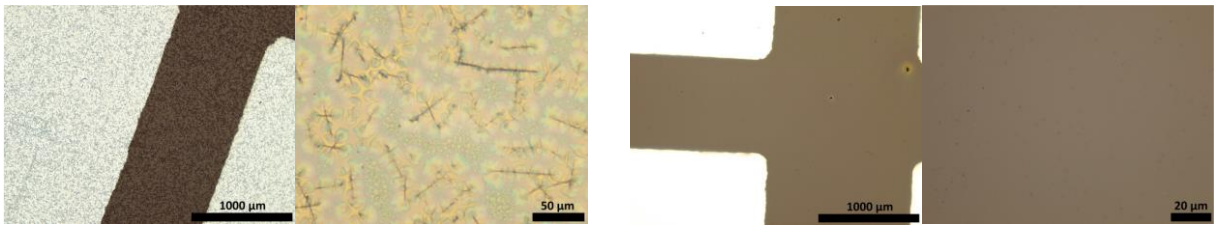


**Figure 29: Light microscope images of the $Et_2Si$-PDI (left) and $Ph_2Si$-PDI (right) solar cells.**

With the integrated area under each EQE also the $J_{SC}$ could be calculated. In Table 5 the $J_{SC}$ values from the EQE are compared with the $J_{SC}$ values from the J-V measurement. While the values for $Cl_4$-PDI and $Et_2$Si-PDI are quite close to the J-V measurement, the other three are much higher when determined by the EQE.

**Table 5: Comparison between the measured $J_{SC}$ and the $J_{SC}$ values calculated from the EQE.**

| Acceptor | $J_{SC}$ (before EQE) [mA/cm$^2$] | $J_{SC}$ (after EQE) [mA/cm$^2$] | $J_{SC}$ (integrated) [mA/cm$^2$] |
|---|---|---|---|
| **PDI** | -3.74 | -3.71 | -4.41 |
| **$Br_2$-PDI** | -3.87 | -4.07 | -5.38 |
| **$Cl_4$-PDI** | -2.71 | -2.93 | -1.99 |
| **$Et_2$Si-PDI** | -5.76 | -6.15 | -5.68 |
| **$Ph_2$Si-PDI** | -3.96 | -3.56 | -5.58 |

That phenomena were further investigated by measuring the three solar cells at different light intensities. The measurement showed that the solar cell function better under low light intensity than under high light intensity. What explains the higher value for $J_{SC}$ from the EQE, because this is carried out under lower intensity than the J-V measurement. For the $Ph_2$Si-PDI $J_{SC}$ values of -4.23 (100%) and 5.75 mA/cm$^2$ (10%) were obtained. Which corresponds to an increase of around 36%. Compounds PDI and $Br_2$-PDI exhibit an even higher increase of 60% and 80%.

# 3 Experimental

## 3.1 Chemicals and Materials

Table 6 shows a summary of all chemicals and materials, their supplier and purity grade. Unless otherwise stated the chemicals were used as received without any purification steps.

**Table 6: List of Chemicals and Materials with their purity grade and supplier.**

| Chemical | Purity Grade and Description | Supplier |
|---|---|---|
| acetone | ≥99% | Sigma Aldrich |
| bromine | >99% | MERCK-Schuchardt |
| cyclohexane | ≥99.5% | VWR Chemicals |
| dichloromethane | >99.8% | Fisher Chemical |
| 2,6-diisopropylaniline | Tech, 90% | Sigma Aldrich |
| diethylsilane | 97+% | Alfa Aesar |
| ethanol | 96% | |
| ethanolamin | ≥99% | Sigma Aldrich |
| hydrochloric acid | 37% | VWR Chemicals |
| imidazole | 99% | Abcr |
| iodine | >99.5% | Fluka |
| ITO coated glass | 15 Ω | Luminescence Technology |
| | 15x15x1.1mm | Corp |
| 2-methoxy ethanol | anhydrous 99.8% | Sigma Aldrich |
| $MoO_3$ | 99.98% | Sigma Aldrich |
| $Na_2SO_4$ | ≥99% | Roth |
| PTCDA | 97% | Sigma Aldrich |
| propionic acid | 99% | Abcr |
| potassium acetate | 98% | Sigma Aldrich |
| silicagel | 0.06-0.2 mm | Macherey-Nagel |
| silver | 99.99% | Kurt J. Lesker |
| sulfuric acid | ≥95% | Fisher Chemical |
| tetrakis | 99.9% | Abcr |
| zinc acetate dihydrate | ≥99.5% | Fluka |

The 2,6-diisopropylaniline was purified by vacuum distillation before use. The potassium acetate was dried in a vacuum drying closet for 30 hours at 100°C before use.

## 3.2 Characterisation

### 3.2.1 NMR spectroscopy

The $^{1}H$ and $^{13}C$ NMR spectroscopy was performed on a Bruker Avance spectrometer operating at 300($^{1}H$) and 75($^{13}C$) MHz. Deuterated chloroform with 0.03% TMS was used to dissolve the samples. The spectra were calibrated regarding the TMS signal at 0 ppm. Peak shapes are described as: s (singlet), bs (broad singlet), d (doublet), t (triplet), m (multiplet). Coupling constants are given in Hz.

### 3.2.2 Thin layer chromatography

For thin layer chromatography silica gel 60 $F_{254}$ on aluminium sheets was used. No visualization method was needed.

### 3.2.3 Thermogravimetric analysis (TGA)

TGA measurements were performed Netzsch Jupiter STA 449C. All measurements were done under He-atmosphere with a flow rate of 50 mL/min and a temperature range of 20-550°C with a heating rate of 10 °C/min. The measurements were performed by Josefine Hobisch (TU Graz). The temperature after 5% mass loss occurred was used for comparison among the compounds.

### 3.2.4 Optical characterisation

For measuring the UV-VIS spectra a UV-1800 Spectrometer from Shimadzu was used. The absorption spectra were recorded in a range of 350 to 1000 nm. The optical bandgaps were determined by using the onset of the absorption spectra. For the film measurements the solutions were spin coated on acetone precleaned glass substrates with 1000 rpm.

The fluorescence measurement was performed on a Fluorolog (Jobin Yvon) from HORIBA. Fluorescence orange (www.kremer-pigmente.com) dissolved in chloroform was used as

reference for all perylene compounds. For the vio compound 3,3-Diethylthiadicarbocyaniniodid dissolved in ethanol was used as reference. Compounds PDI, $Br_2$-PDI, $Cl_4$-PDI were exited at 485 nm, the emission was measured from 500-800 nm with a slit width of 1 nm. Compounds $Et_2Si$-PDI and $Ph_2Si$-PDI were exited at 492 nm, the emission was measured from 502-800 nm with a slit width of 1 nm. The vio compound was exited at 570 nm, the emission was measured from 585-900 nm with a slit width of 1 nm.

### 3.2.5 J-V measurement

For the measurement the substrates were irradiated with artificial sunlight produced by a Dedolight DLH400D lamp. The illumination was set to an intensity of 100 mW $cm^{-2}$ to mimic sunlight of AM 1.5 G. Each solar cell was measured with a shadow mask, which reduced the irradiated area to 0.070226 $cm^2$. The J-V-curves were recorded with a Keithley 2400 source meter combined with a custom-made LabVIEW software. The J-V-curve was measured at a voltage range of -500 mV to 1500 mV with a delay of 100 ms, a maximum compliance of 500 mA. The obtained J-V characteristics ($V_{OC}$, $J_{SC}$, FF, PCE) were averaged over the best 5 cells.

### 3.2.6 Layer Thickness and Roughness

The layer thickness and roughness of the produced solar cells were measured by using a Dektak XT surface profilometer by Bruker. The stylus force was 3 mg and the measured length of 1000 µm was obtained with a speed of 100 µ $s^{-1}$.

### 3.2.7 External quantum efficiency (EQE)

The EQE was measured by using a monochromator MuLTImode4 equipped with a Xenon lamp provided by AMKO and a Keithley 2400 SourceMeter. A photodiode was used for the calibration and the spectra were recorded in a range of 380-730 nm.

## 3.3 Solar cell preparation

The solar cells were built in the inverted device architecture illustrated in Figure 3. All solar cells were built in the same manner: ITO/ZnO/active layer/$MoO_3$/Ag

### 3.3.1 Substrate preparation

At first the ITO coated glass substrates (15 Ω resistance) were cleaned with acetone and a microfiber cloth (kimtech) to get rid of primary impurities. In the next step the substrates were submerged in an isopropanol solution and treated with ultrasonic bath (60 min, 40 °C, VWR ultrasonic cleaner). After drying with a nitrogen stream the substrate were etched by an oxygen plasma etching machine (FEMTO, Diener Electronic) for 3 min. For the next steps the activated substrates were transferred into a glovebox (LABmaster dp, MBraun) with $N_2$ atmosphere.

### 3.3.2 Electron transport layer

ZnO was used as electron transport layer. Therefore, zinc acetate dihydrate (500 mg) was mixed with 2-methoxy-ethanol (5 mL) and ethanolamine (150 µL) in a small vial. After stirring for 12 hours under ambient air it was transferred into the glove box. The ZnO solution was always filtered (0.45 µm syringe filter) before use. The ZnO solution was applied onto the substrate by spin coating (Model WS 650 MZ-23NPPB) 35 µL of the solution at 4000 rpm for 30 seconds and an acceleration of 2000. Afterwards the substrates were annealed at 150 °C for 15 min under ambient air.

### 3.3.3 Active layer

Initially the perylenediimide acceptor was dissolved in chlorobenzene (12 – 15 mg/mL) and stirred for 1-2 hours till it was completely dissolved. Then the solution was added to the solid polymer (PBDB-T or P3HT) with a donor:acceptor ratio 1:1 and stirred for one hour at 60 °C. Subsequently the blend was stirred overnight at room temperature. On the next day 20 µL of the polymer-acceptor blend were used for spin coating each substrate (500 accel, 30 sec). After the initial spin coating step with varying rotation speed a second one followed (4000 rpm, 2000 accel, 5 sec) to ensure a dry substrate layer.

### 3.3.4 Solvent Annealing

For the solvent annealing the spin coated substrate was placed on a glass petri dish. Next to the substrate a drop of the used solvent (chlorobenzene) was placed without touching the substrate. After covering the petri dish with another petri dish, it was placed on the heating plate and annealed at varying temperatures for 5 min.

### 3.3.5 Hole transport layer and top Electrode

$MoO_3$ (10 nm) was used as hole transport layer. It was applied by thermal deposition with a rate of 0.1 Å/s. For the top electrode silver (100 nm) was deposited with a rate of 0.1 Å/s for the first 10 nm and 1 Å/s for the rest. Thermal deposition was performed in an evaporation chamber (MB EVAP, MBraun) inside the glovebox at a vacuum level of approximately $1x10^{-5}$ mbar. The deposition rate and final thickness was monitored with an SQM-160 Deposition Rate/Thickness Monitor by Inficon. A mask was used to limit the deposited area to 0.09 $cm^2$ for every cell on each substrate.

## 3.4 Synthesis

### 3.4.1 Synthesis of $N^1$-$N^2$-(2,6-diisopropylphenyl)-perylene-3,4,9,10-tetracarboxylicdiimide

Literature:[53]

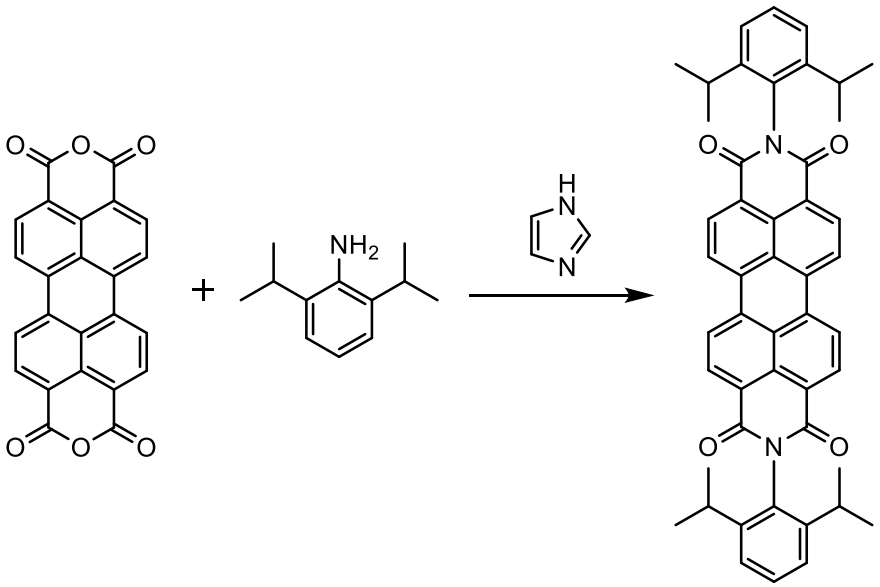


**PTCDA** **PDI**

Perylene-3,4,9,10-tetracarboxydianhydride (PTCDA) (1.0 g; 2.55 mmol; 1 eq) was mixed with 2,6-diisopropylaniline (2.0 g; 0.110 mol; 4 eq) and imidazole (7.5 g) in a round bottom flask equipped with a reflux condenser. The reaction was heated to 180 °C under $N_2$ atmosphere, for 44 hours. Afterwards the reaction mixture was cooled down to room temperature, 50 mL ethanol and 60 mL of 2 M HCl was added and the mixture was stirred for 3 hours. Then the

precipitate was filtered and washed with deionized water. After purification with a column chromatography ($SiO_2$, DCM) a brown-red solid was obtained as product.

Yield: 1.187 g (66%)

$R_f$= 0.38 (DCM)

$^1$H NMR (300 MHz, $CDCl_3$) $\delta_{ppm}$: 8.80 (d, *J* = 8.0 Hz, 2H), 8.75 (d, *J* = 8.0 Hz, 2H), 7.51 (t, *J* = 7.7 Hz 2H), 7.36 (d, *J* = 7.7 Hz, 4H), 2.76 (m, 4H) 1.19 (d, *J* = 7.0 Hz, 24H) $^{13}$C NMR (75 MHz, $CDCl_3$) $\delta_{ppm}$: 163.5, 145.7, 135.1, 132.2, 130.6, 129.8, 126.9, 124.2, 123.5, 123.37, 29.3, 24.0

UV-Vis ($CHCl_3$) $\lambda_{max}$ nm (rel. in.): 527 (1), 490 (0.59), 459 (0.23)

## 3.4.2 Synthesis of 1,7(6)-Dibromoperylene-3,4,9,10-tetracarboxydianhydride

Literature: [66]

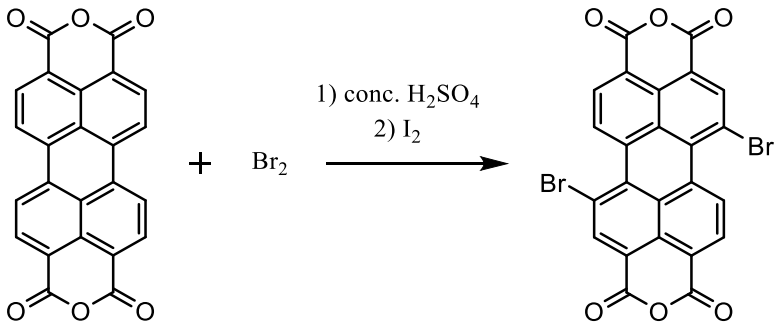


**PTCDA** **2**

Perylene-3,4,9,10-tetracarboxydianhydride (PTCDA) (5.0 g; 12.745 mmol; 1 eq) was suspended in 150 mL conc. sulfuric acid in a three neck round bottom flask equipped with a reflux condenser. The mixture was stirred for 2 hours at 55 °C. After adding iodine (258.8 mg; 1.019 mmol; 0.08 eq) the reaction mixture was stirred for 2.5 hours at 82 °C. When the reaction mixture cooled down to room temperature, bromine (3.9 mL, 76.468 mmol, 6 eq) was slowly added with a syringe. The reaction mixture was first stirred at 95 °C for 2 hours and then at room temperature over the weekend. The raw product was precipitated by the addition of 500 mL deionized water, filtered of and washed with deionized water until the wash solution reached a neutral pH. A red solid product with quantitative yield was obtained.

Because of its insolubility the product was used for further reactions without any characterization or purification step.

### 3.4.3 Synthesis of $N^1$-$N^2$-(2,6-iisopropylphenyl)-1, 7 dibromoperylene-3,4,9,10-tetracarboxylicdiimide

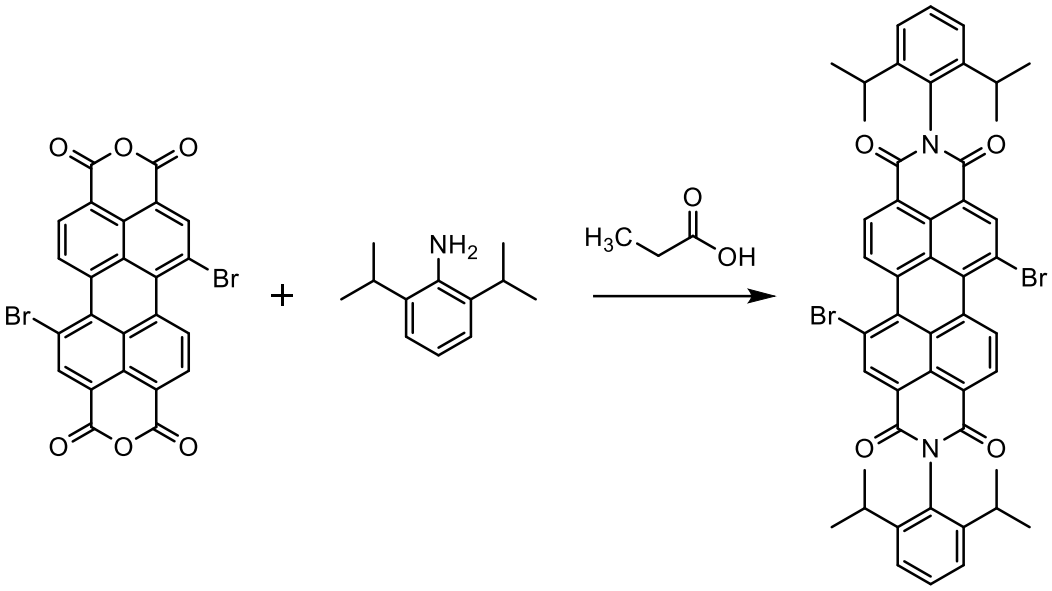


**2** **$Br_2$-PDI**

The reaction mixture of 1,7(6)-Dibromoperylene-3,4,9,10-tetracarboxydianhydride (7.0 g, 0.0127 mol, 1 eq) was dissolved in 370 mL propionic acid and 2,6-diisopropylaniline (9.6 mL, 0.0509 mol, 4 eq). A two neck round bottom flask equipped with a reflux condenser was used. The reaction mixture was stirred for 24 hours at reflux and under $N_2$ atmosphere. After cooling down, the reaction mixture was treated with 500 mL deionized water and the precipitate was filtered of. Afterwards the product was extracted with dichloromethane, dried over $Na_2SO_4$ and the solvent was evaporated under reduced pressure. The product was further purified by column chromatography ($SiO_2$, DCM) resulting in a red-orange solid.

Yield: 1.843 g (17%)

$R_f$= 0.68 (DCM)

$^1$H NMR (300 MHz, $CDCl_3$) $\delta_{ppm}$: 9.57 (d, *J* = 8.1 Hz, 2H), 9.03 (s, 2H), 8.81 (d, *J* = 8.1 Hz 2H), 7.52 (t, *J* = 7.7 Hz, 2H), 7.37 (d, *J* = 7.7 Hz, 4H) 2.74 (m, 4H) 1.19 (d, *J* = 7.0 Hz, 24H)
$^{13}$C NMR (75 MHz, $CDCl_3$) $\delta_{ppm}$: 163.1, 162.6, 145.7, 144.2, 138.5, 133.5, 133.3, 130.7, 129.9, 129.6, 128.8, 127.7, 124.3, 123.2, 123.9, 121.1, 29.4, 24.2

UV-Vis ($CHCl_3$) $\lambda_{max}$ nm (rel. in.): 528 (1), 491 (0.68), 459 (0.27)

### 3.4.4 Synthesis of $N^1$-$N^2$-(2,6-diisopropylphenyl)-1,6,7,12 tetrachloroperylene-3,4,9,10-tetracarboxylicdiimide

Literature:[67]

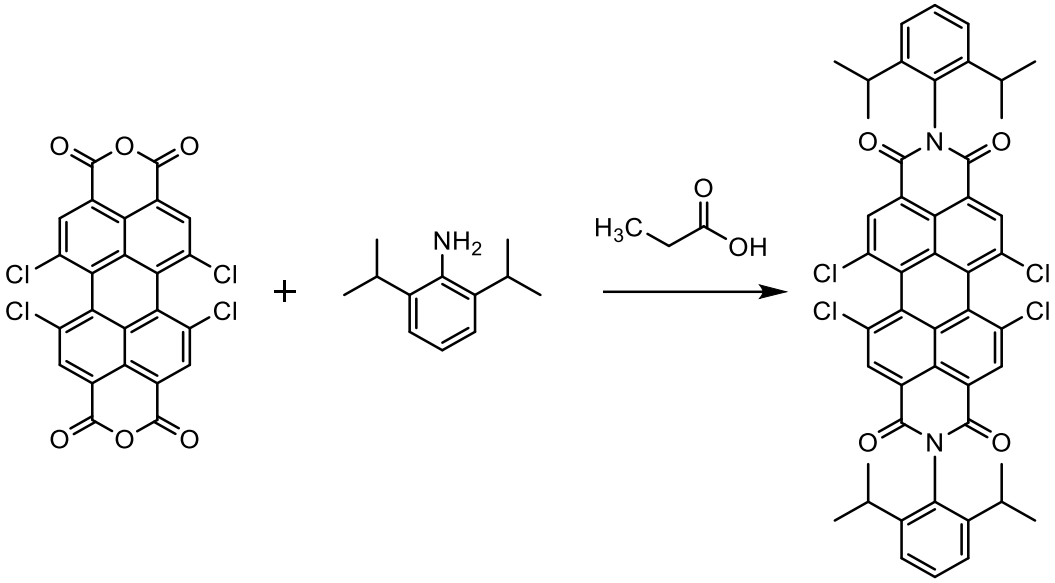


1,6,7,12-Tetrachloroperylene-3,4,9,10-tetracarboxydianhydride (6.0 g, 0.0114 mmol, 1 eq) was dissolved in 300 mL propionic acid and 2,6-diisopropylaniline (8.5 mL, 0.0448 mol, 4 eq). Therefore, a two neck round bottom flask equipped with a reflux condenser was used. The reaction mixture was stirred for 24 hours at reflux and under $N_2$ atmosphere. After cooling down, the reaction mixture was treated with 500 mL deionized water and the precipitate was filtered of. The precipitate was first washed with deionized water, then with $H_20$/MeOH (50:50). Afterwards the product was extracted with dichloromethane, dried over $Na_2SO_4$ and the solvent was evaporated under reduced pressure. The product was further purified by column chromatography ($SiO_2$, DCM) resulting in a orange solid.

Yield: 7.896 g (82%)

$R_f$= 0.87 (DCM)

$^{1}$H NMR (300 MHz, $CDCl_3$) $\delta_{ppm}$: 8.78 (s, 4H), 7.53 (t, *J* = 7.8 Hz, 2H), 7.38 (d, *J* = 7.7 Hz, 4H), 2.72 (m, 4H), 1.19 (d, *J* = 7.0 Hz, 24H) $^{13}$C NMR (75 MHz, $CDCl_3$) $\delta_{ppm}$: 162.4, 145.7, 135.7, 133.5, 131.8, 130.1, 129.9, 128.9, 124.3, 124.0, 123.3, 29.3, 24.1

UV-Vis ($CHCl_3$) $\lambda_{max}$ nm (rel. in.): 521 (1), 487 (0.69), 428 (0.28)

### 3.4.5 Synthesis of Synthesis of *N*$^{1}$-*N*$^{2}$-(2,6-diisopropylphenyl)-1,12 diethylsilane-perylene-3,4,9,10-tetracarboxylicdiimide

Literature:[46]

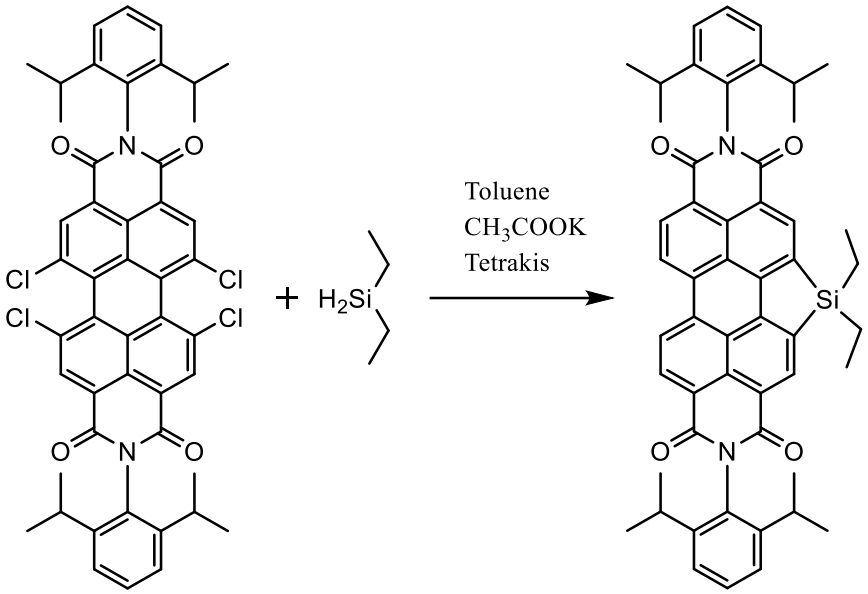


**$Cl_4$-PDI** **$Et_2Si$-PDI**

1,6,7,12-tetrachloroperylenediimide (1.0 g, 1.178 mol, 1 eq) were dissolved in 33 mL dry toluene in a Schlenk flask. After adding tetrakis (40 mg, 0.178 mmol, 15%eq), dry potassium acetate (578 mg, 5.89 mol, 5 eq) and diethylsilane (1.1 mL, 8.245 mol, 7 eq) the reaction was stirred under Ar atmosphere at 110 °C for 20 hours. After cooling down to room temperature the reaction mixture was filtered off and washed with dichloromethane. Afterwards the filtrate was concentrated under reduced pressure and the obtained crude product was purified by column chromatography ($SiO_2$, DCM) resulting in a red solid.

Yield: 0.187 g (22%)

$R_f$= 0.46 (DCM)

$^{1}$H NMR (300 MHz, $CDCl_3$) $\delta_{ppm}$: 8.92 (s, 4H), 8.76 (d, *J* = 8.0 Hz, 2H), 8.64 (d, *J* = 8 Hz, 2H) 7.51 (t, *J* = 7.7 Hz, 2H), 7.37 (d, *J* = 7.7 Hz, 4H), 2.79 (m, 4H), 1.20 (m, 28H), 1.09 (m, 6H) $^{13}$C NMR (75 MHz, $CDCl_3$) $\delta_{ppm}$: 164.3, 163.6, 147.4, 145.7, 137.3, 135.8, 135.5, 132.6, 130.9, 129.7, 125.0, 124.5, 124.2, 123.5, 123.3, 122.2, 29.2, 24.1, 7.8, 2.8 $^{29}$Si NMR (100 MHz, $CDCl_3$) $\delta_{ppm}$: 12.9

UV-Vis ($CHCl_3$) $\lambda_{max}$ nm (rel. in.): 548 (1), 509 (0.66), 477 (0.27)

### 3.4.6 Synthesis of Synthesis of *N*$^{1}$-*N*$^{2}$-(2,6-diisopropylphenyl)-1,12 diphenylsilane-perylene-3,4,9,10-tetracarboxylicdiimide

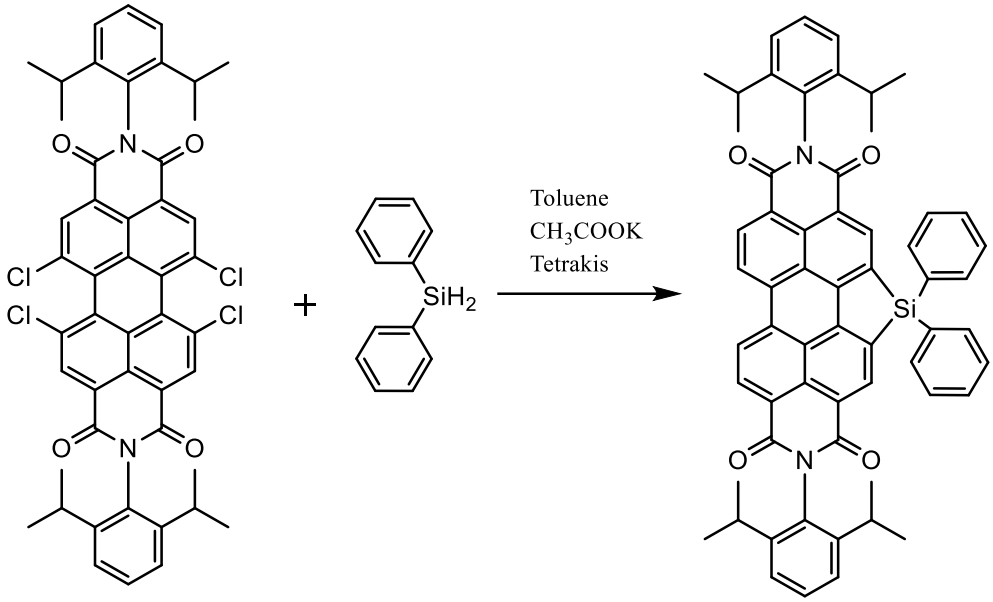


**$Cl_4$-PDI** **$Ph_2Si$-PDI**

1,6,7,12-tetrachloroperylenediimide (0.2 g, 1.178 mol, 1 eq) were dissolved in 33 mL dry toluene in a Schlenk flask. After adding tetrakis (40 mg, 0.178 mmol, 15%eq), dry potassium acetate (578 mg, 5.89 mol, 5 eq) and diphenylsilane (1.1 mL, 8.245 mol, 7 eq) the reaction was stirred under Ar atmosphere at 110 °C for 20 hours. After cooling down to room temperature the reaction mixture was filtered off and washed with dichloromethane. Afterwards the filtrate was concentrated under reduced pressure and the obtained crude product was purified by column chromatography twice: 1) $SiO_2$, DCM; 2) $SiO_2$, CH/EtAc 4:1 resulting in a red solid.

Yield: 0.027 g (11%)

$R_f$= 0.46 (DCM)

$^{1}$H NMR (300 MHz, $CDCl_3$) $\delta_{ppm}$: 9.02 (s, 2H), 8.77 (d, *J* = 8.1 Hz, 2H), 8.65 (d, *J* = 8.1 Hz, 2H) 7.79 (d, *J* = 7.1 Hz, 2H), 7.49 (m, 8H), 7.35 (d, *J* = 7.7 Hz, 4H), 2.77 (m, 4H), 1.18 (m, 24H), $^{13}$C NMR (75 MHz, $CDCl_3$) $\delta_{ppm}$: 164.0, 163.4, 147.7, 145.7, 136.4, 135.9, 135.7, 135.6, 133.0, 131.6, 131.1, 130.8, 129.7, 128.9, 128.3, 125.3, 124.1, 123.6, 123.5, 122.9, 29.8, 29.2, 24.1

UV-Vis ($CHCl_3$) $\lambda_{max}$ nm (rel. in.): 550 (1), 511 (0.66), 476 (0.27)

## 3.4.7 Synthesis of 16,17-Bis(2-ethylhexyloxy)anthra[9,1,2-cde]benzol[rst]pentaphene-5,10-dione

Literature:[56]

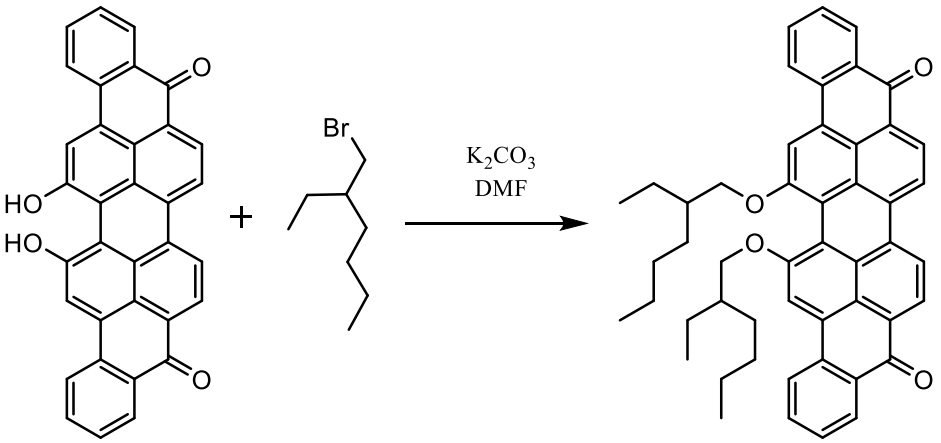


**Vio**

Violanthrone (220 mg, 0.45 mmol, 1 eq) and 125 mg anhydrous potassium carbonate were dissolved with 5.4 mL of dimethylformamide in round bottom flask equipped with a reflux condenser. After that 2-ethylhexylbromide (261 mg, 1.35 mmol, 3 eq) was added and the mixture was stirred for 22 h at 100°C. After the reaction mixture cooled down to room temperature, it was poured into 50 mL of methanol. The dark blueish precipitate was then washed with water and filtered of. Afterwards it was purified by column chromatography ($SiO_2$, $CHCl_3$) resulting in a dark-purple powder with a metallic shine.

Yield: 0.121 g (38%)

$R_f$= 0.13 ($CHCl_3$)

$^{1}$H NMR (300 MHz, $CDCl_3$) $\delta_{ppm}$: 8.52 (d, *J* = 8.2 Hz, 2H), 8.43 (d, *J* = 8.0 Hz, 2H), 8.36 (m, 4H), 8.25 (s, 2H), 7.79 (t, *J* = 7.4 Hz, 2H), 7.56 (t, *J* = 7.4 Hz, 2H), 4.08 (m, 4H), 1.81 (s, 2H)

1.34 (m, 17H), 0.78 (m, 12H) $^{13}$C NMR (75 MHz, $CDCl_3$) $\delta_{ppm}$: 182.9, 156.9, 135.6, 134.2, 133.1, 130.9, 129.4, 128.5, 128.2, 127.6, 127.5, 126.9, 123.6, 123.2, 122.5, 117.4, 114.4, 40.5, 30.6, 29.3, 23.9, 23.1, 14.2, 11.3

UV-Vis ($CHCl_3$) $\lambda_{max}$ nm (rel. in.): 647 (1)

## 3.5 Computations

DFT calculations were performed by using Gaussian 09 Revision D.01 from Gaussian Inc.[68] The structures were first drawn with ChemDraw and the geometry was pre optimized in ChemDraw3D. B3LYP functional was used for every calculation while the basis set varied between 6-31G*, 6-31+G* or 3-21G.

# 4 Summary and Outlook

Non-fullerene acceptors are of constant interest because of their various advantages and steadily increasing power conversion efficiencies. One aspect of current research is the dielectric constant of non-fullerene acceptors and its influence on the solar cell performance. Therefore, perylene diimide based structures with various substituents in the bay position were synthesized and their influence on the optical and energetical properties examined. The experimental characterisation was assisted by DFT calculations providing information including the dipole moment. With them a possible increase in the dielectric constant could be estimated. Subsequently, the acceptors were tested in organic solar cells using an inverted device structure: ITO/ZnO/BHJ/$MoO_3$/Ag.

In summary, it was shown that by introducing a silicon substituent into the perylene structure an increase of the dipole moment could be observed. The obtained solar cell data indicates a relationship between the dipole moment and the solar cell performance. As a result, the acceptors with increased dipole moment lead to an enhanced solar cell performance. Expressed in numbers, compounds $Et_2$Si-PDI and $Ph_2$Si-PDI exhibit maximum power conversion efficiencies of 2.42 and 1.55%, respectively. This represents, especially for compound $Et_2$Si-PDI, a strong increase in efficiency when compared with the PDI, the perylene without any substituents. Of course, the influence of the dipole moment has to be verified by further measurements like the dielectric constant of the acceptors. Besides that, the silicon substituents are sterically more demanding, which could influence the intermixing with the donor and the morphology of the active layer and therefore also strongly influencing the solar cell performance. Moreover, each solar cell setup has to be further optimized to reach its maximum potential, before a clear relationship between the dipole moment and the solar cell performance can be stated. Although there is no big difference regarding optical and energetical properties, the two silicon compounds show strong difference in power conversion efficiencies. This can be attributed to the different substituents on the silicon having a strong impact on the intermixing with the polymer and the resulting morphology. This statement is confirmed by the light microscopy images showing clear and smooth active layers for the $Ph_2$Si-PDI compound while active layers of $Et_2$Si-PDI appear rougher and full of particles. Those acicular crystallin particles seem to be very beneficial for the solar cell performance. Compound PDI exhibits a maximum efficiency of 1.38%. The two halogenated compounds $Br_2$-PDI and $Cl_4$-PDI achieved

efficiencies of 1.06 and 0.71% each. $Cl_4$-PDI exhibits a slightly increased dipole moment of 0.45 Debye, probably caused by the higher electron negativity of the chlorine atom. It has to be pointed out that the lower efficiency of compound $Cl_4$-PDI is mainly a result of the lower $V_{OC}$. This result fits very well to the calculated energy levels in which $Cl_4$-PDI has the lowest lying LUMO level. The lower lying LUMO level minimizes the gap between the LUMO of the acceptor and the HOMO of the donor, which corresponds to the $V_{OC}$. Of course, the calculated $V_{OC}$ is not equal to the measured one, because there are also radiative and non-radiative losses which reduce it. But it can be clearly seen how the $V_{OC}$ decreases from PDI>$Br_2$-PDI>$Cl_4$-PDI, while the energy levels also decline. The measured EQE displays the highest quantum efficiency of over 40% for $Ph_2$Si-PDI, while the others are around 35%. Except $Cl_4$-PDI which shows an EQE of 10%. These values reflect the measured J-V very good. The J-V measurement at different light intensities displays that compounds PDI, $Br_2$-PDI and $Ph_2$Si-PDI achieve higher $J_{SC}$ values under low light intensities.

Furthermore, TGA measurement showed how the thermal stability of the perylene decreases when substituents are introduced. Giving PDI the highest thermal stability of 478 °C followed by $Et_2$Si-PDI with 448 °C. $Br_2$-PDI and $Cl_4$-PDI exhibit a thermal stability of 393 °C and 443 °C, respectively. Due to the high thermal stability also high annealing temperatures could be used. Like for $Et_2$Si-PDI which was annealed at 220 °C. $Br_2$-PDI and $Cl_4$-PDI were annealed with 170 °C and 120 °C, respectively.

The obtained solar cells show beneficial impact of compounds, with increased dipole moment on the solar cell performance. Therefore, it is suggested for further studies to investigate other compounds with increased dipole moment. For example, the two perylene diimides with the cyano and thiocyano groups presented in Table 2. Especially the thiocyano substituted perylene exhibits a very high dipole moment of 3.15 Debye, making it a promising candidate for further investigations.

In this work, the presented solar cell devices should be further optimized by varying the donor acceptor ratio or by adding additives to assess the full potential of these acceptors. Furthermore, their dielectric constant should be determined.

# 5 Appendix

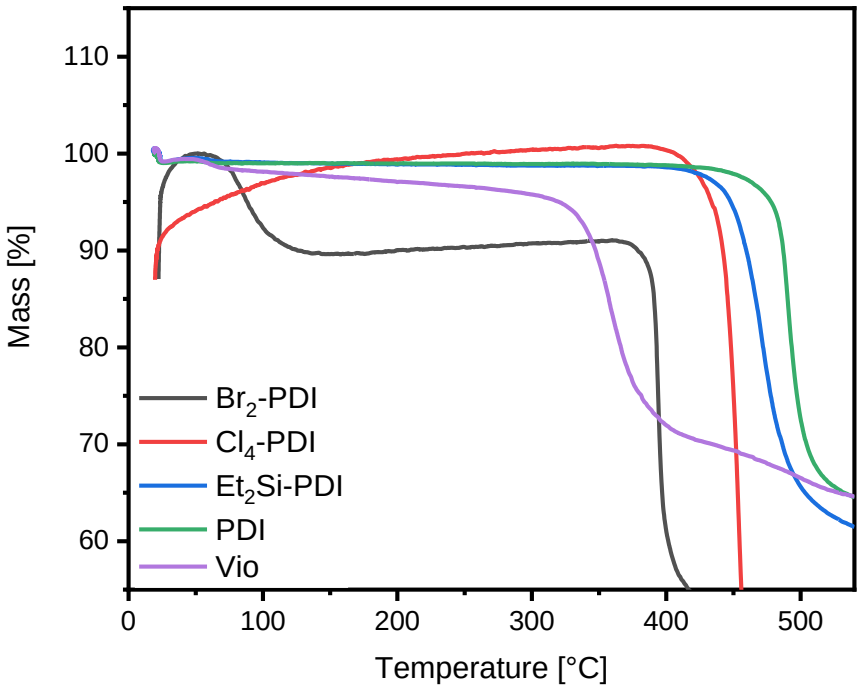


**Figure 30: TGA curves of compounds PDI, $Br_2$-PDI, $Cl_4$-PDI, $Et_2$Si-PDI, vio .**

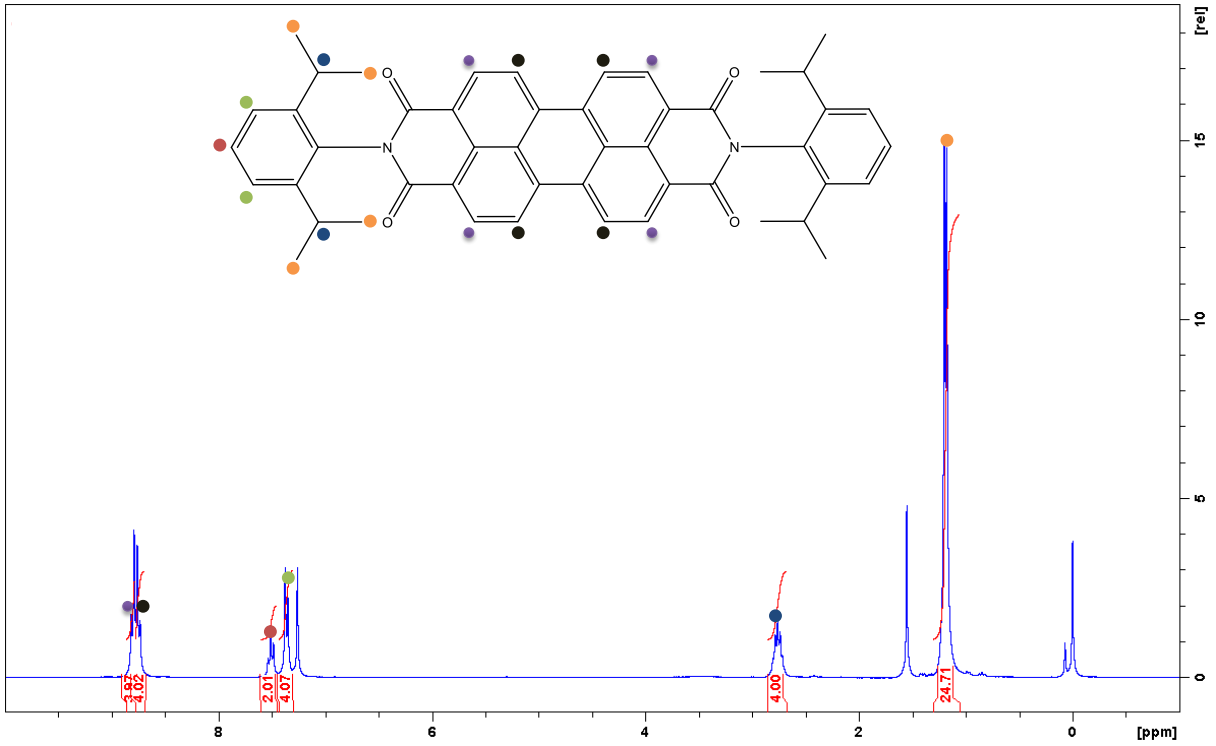


**Figure 31: $^1$H-NMR spectrum of compound PDI.**

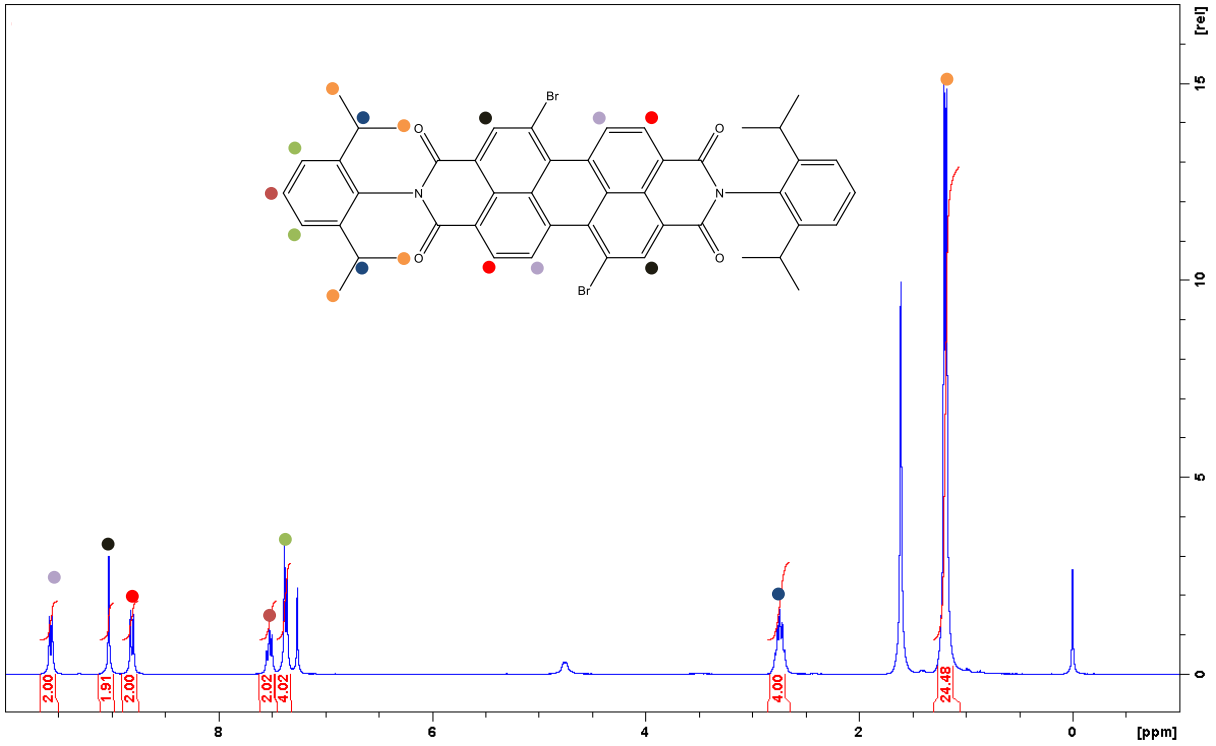


**Figure 32: $^{1}$H-NMR spectrum of compound $Br_2$-PDI.**

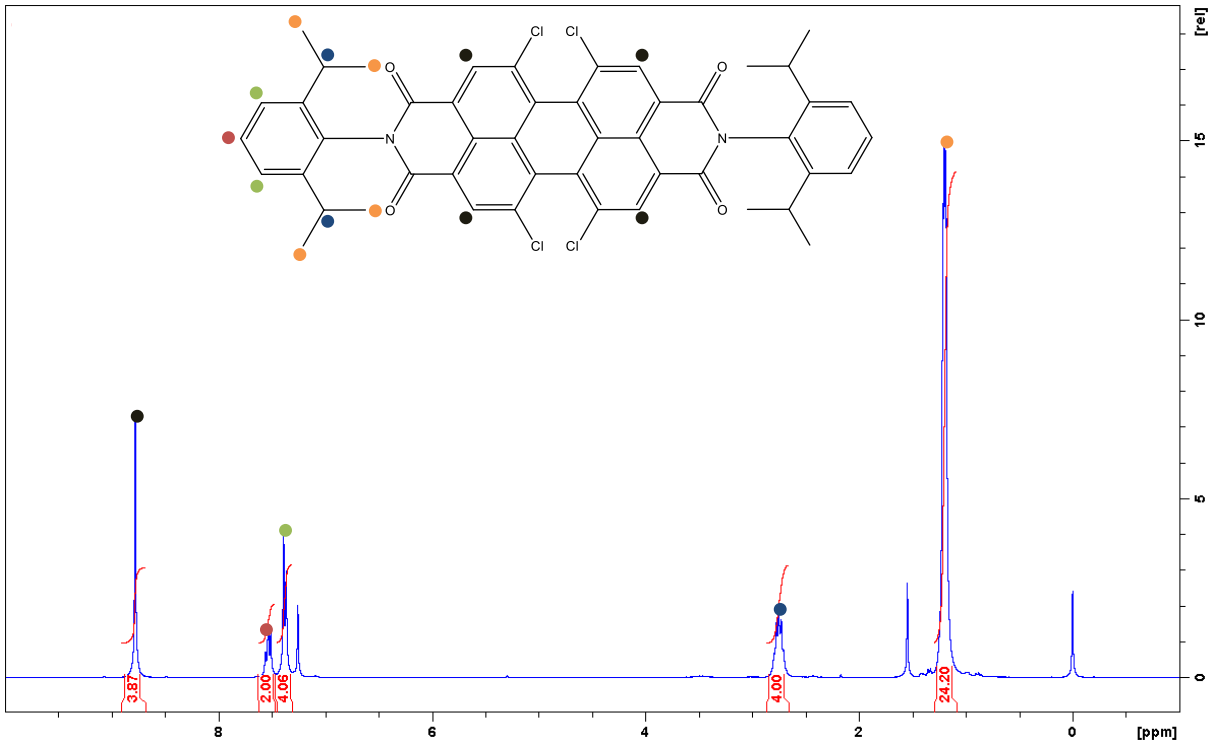


**Figure 33: $^{1}$H-NMR spectrum of compound $Cl_4$-PDI.**

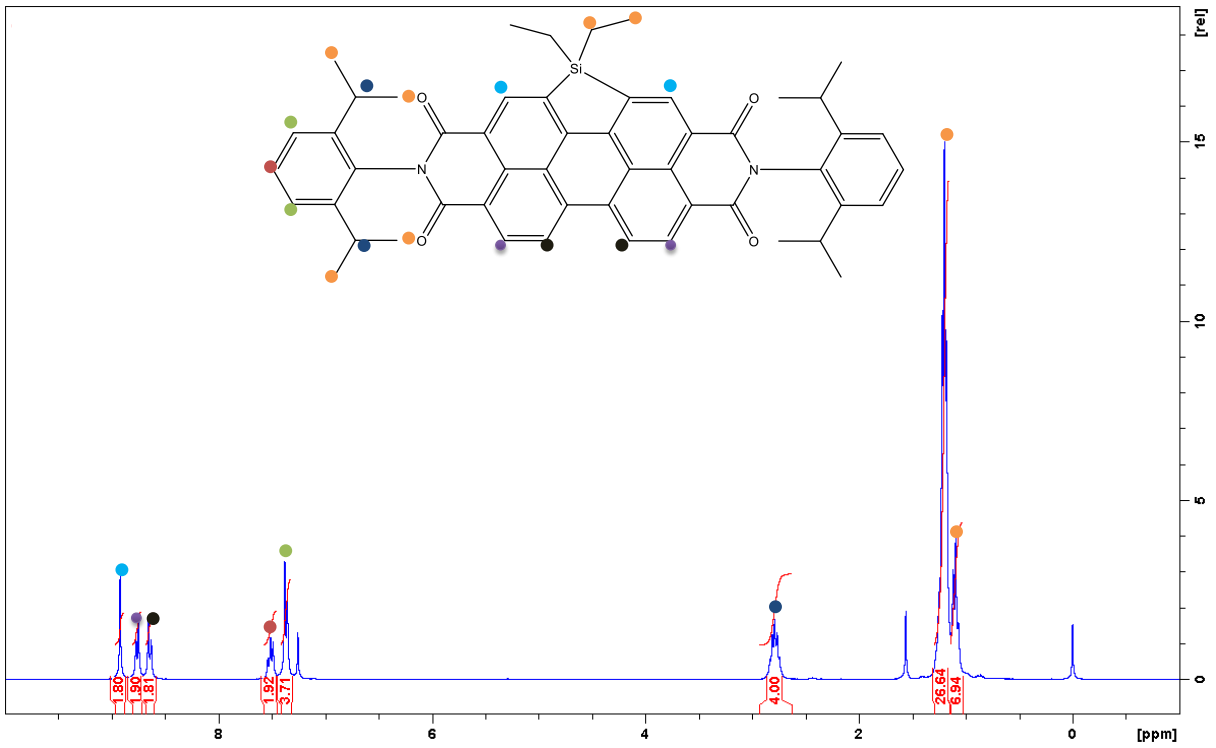


**Figure 34: $^{1}$H-NMR spectrum of compound $Et_2$Si-PDI.**

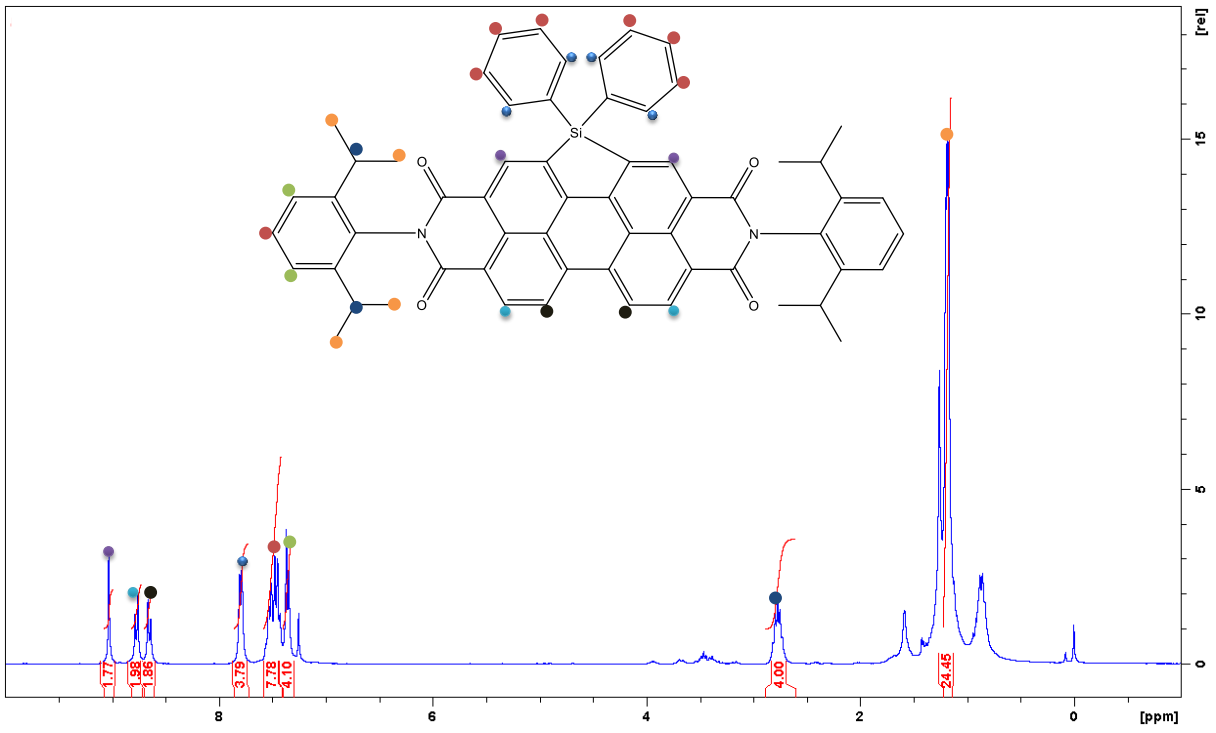


**Figure 35: $^{1}$H-NMR spectrum of compound $Ph_2$Si-PDI.**

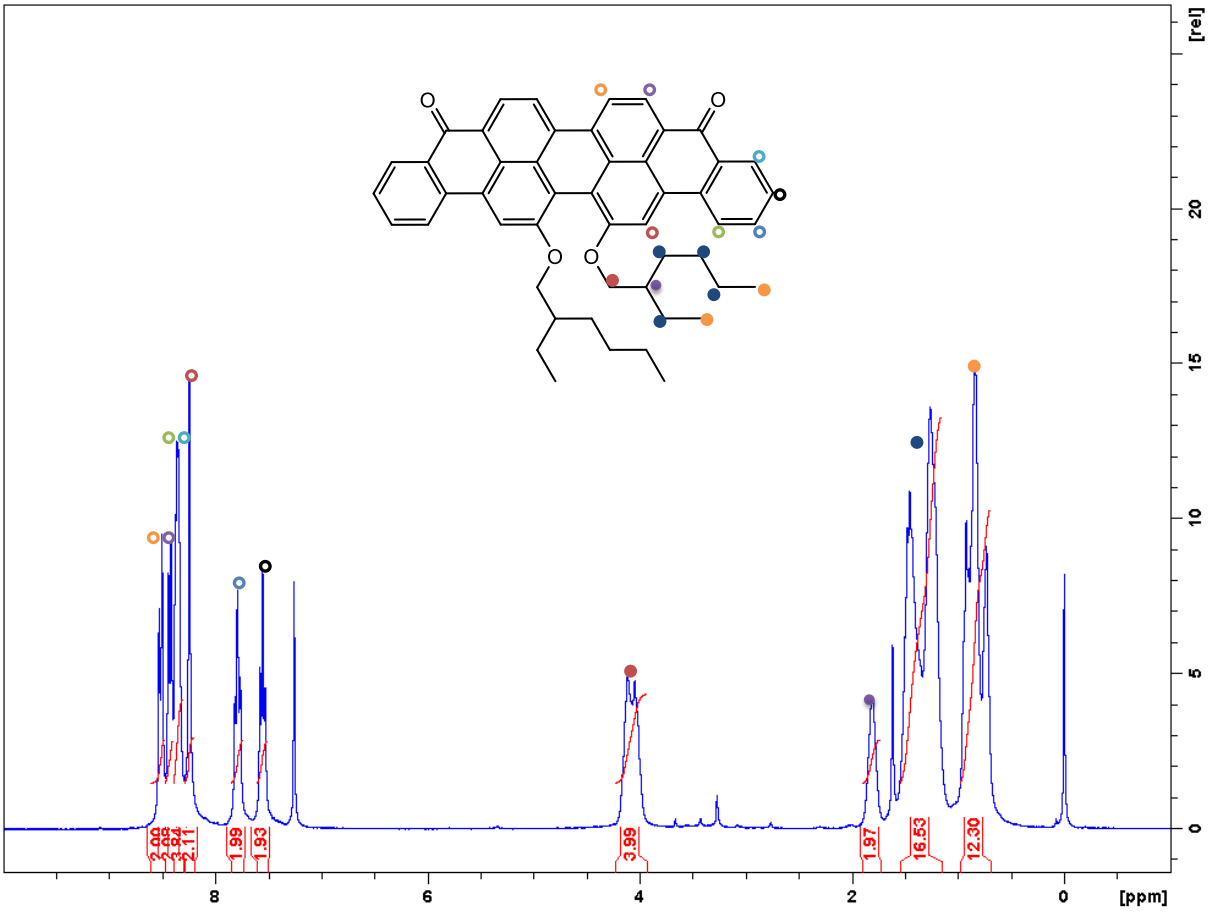


**Figure 36: $^{1}$H-NMR spectrum of compound vio.**

## 5.1 Index of figures

## 5.2 Index of tables



## 5.3 References

1. https://www.iea.org/newsroom/news/2019/march/global-energy-demand-rose-by-23-in-2018-its-fastest-pace-in-the-last-decade.html. (Accessed: 11th September 2019)

2. https://www.ren21.net/gsr-2019/chapters/chapter_01/chapter_01/. (Accessed: 28th August 2019)

3. Azarpour, A., Suhaimi, S., Zahedi, G. & Bahadori, A. A review on the drawbacks of renewable energy as a promising energy source of the future. *Arab. J. Sci. Eng.* **38**, 317–328 (2013).

4. Blandford, R. & Watkins, M. This Month in Physics History: April 25, 1954: Bell Labs Demonstrates the First Practical Silicon Solar Cell. *APS News* **18**, 2 (2009).

5. Kibria, M. T., Ahammed, A., Sony, S. M. & Hossain, F. A Review : Comparative studies on different generation solar cells technology. *Int. Conf. Environ. Asp. Bangladesh* 51–53 (2014).

6. Ranabhat, K. *et al.* An introduction to solar cell technology. *J. Appl. Eng. Sci.* **14**, 481–491 (2016).

7. Nelson, J. Polymer : fullerene bulk heterojunction solar cells The efficiency of solar cells made from a conjugated polymer blended. *Mater. Today* **14**, 462–470 (2011).

8. Wang, Y. *et al.* All-Small-Molecule Organic Solar Cells Based on Pentathiophene Donor and Alkylated Indacenodithiophene-Based Acceptors with Efficiency over 8%. *ACS Appl. Energy Mater.* **1**, 2150–2156 (2018).

9. Wang, G., Melkonyan, F. S., Facchetti, A. & Marks, T. J. All-Polymer Solar Cells: Recent Progress, Challenges, and Prospects. *Angew. Chemie - Int. Ed.* **58**, 4129–4142 (2019).

10. Peumans, P., Yakimov, A. & Forrest, S. R. Small molecular weight organic thin-film photodetectors and solar cells. *J. Appl. Phys.* **93**, 3693–3723 (2003).

11. Nunzi, J. M. Organic photovoltaic materials and devices. *Comptes Rendus Phys.* **3**, 523–542 (2002).

12. Sekine, N., Chou, C. H., Kwan, W. L. & Yang, Y. ZnO nano-ridge structure and its application in inverted polymer solar cell. *Org. Electron. physics, Mater. Appl.* **10**, 1473–1477 (2009).

13. Hau, S. K. *et al.* Air-stable inverted flexible polymer solar cells using zinc oxide nanoparticles as an electron selective layer. *Appl. Phys. Lett.* **92**, 2006–2009 (2008).

14. Dyer-Smith, C. & Nelson, J. *Chapter IE-2 – Organic Solar Cells*. *Practical Handbook of Photovoltaics* (Elsevier Ltd, 2012). doi:10.1016/B978-0-12-385934-1.00016-7

15. Shockley, W. & Queisser, H. J. Detailed balance limit of efficiency of p-n junction solar cells. *J. Appl. Phys.* **32**, 510–519 (1961).

16. Ameri, T., Dennler, G., Lungenschmied, C. & Brabec, C. J. Organic tandem solar cells: A review. *Energy Environ. Sci.* **2**, 347–363 (2009).

17. Yan, C., Barlow, S., Jen, A. K.-Y. & Marder, S. Non-fullerene acceptors for organic solar cells Non-Radiative Recombination in Organic Solar Cells Unprecedented highest EO coefficient of 216 pm/V for electro-optic polymer/TiO2 multilayer slot waveguide modulators. *Nat. Publ. Gr.* **3**, 1–19 (2018).

18. Venkateswararao, A., Liu, S. W. & Wong, K. T. Organic polymeric and small molecular electron acceptors for organic solar cells. *Mater. Sci. Eng. R Reports* **124**, 1–57 (2018).

19. Qi, B. & Wang, J. Fill factor in organic solar cells. *Phys. Chem. Chem. Phys.* **15**, 8972–8982 (2013).

20. Günes, S., Neugebauer, H. & Sariciftci, N. S. Conjugated polymer-based organic solar cells. *Chem. Rev.* **107**, 1324–1338 (2007).

21. Tang, C. W. Two-layer organic photovoltaic cell. **183**, (2004).

22. Spanggaard, H. & Krebs, F. C. A brief history of the development of organic and polymeric photovoltaics. *Sol. Energy Mater. Sol. Cells* **83**, 125–146 (2004).

23. Cui, Y. *et al.* Over 16% efficiency organic photovoltaic cells enabled by a chlorinated acceptor with increased open-circuit voltages. *Nat. Commun.* **10**, 1–8 (2019).

24. Yuan, J. *et al.* Single-Junction Organic Solar Cell with over 15% Efficiency Using Fused-Ring Acceptor with Electron-Deficient Core. *Joule* **3**, 1140–1151 (2019).

25. Mizuguchi, J. & Tojo, K. Electronic structure of perylene pigments as viewed from the crystal structure and excitonic interactions. *J. Phys. Chem. B* **106**, 767–772 (2002).

26. Dittmer, J. J., Marseglia, E. A. & Friend, R. H. Electron trapping in dye/polymer blend photovoltaic cells. *Adv. Mater.* **12**, 1270–1274 (2000).

27. Sun, J. P., Hendsbee, A. D., Dobson, A. J., Welch, G. C. & Hill, I. G. Perylene diimide based all small-molecule organic solar cells: Impact of branched-alkyl side chains on solubility, photophysics, self-assembly, and photovoltaic parameters. *Org. Electron. physics, Mater. Appl.* **35**, 151–157 (2016).

28. Chen, Y., Zhang, X., Zhan, C. & Yao, J. In-depth understanding of photocurrent enhancement in solution-processed small-molecule: Perylene diimide non-fullerene

organic solar cells. *Phys. Status Solidi Appl. Mater. Sci.* **212**, 1961–1968 (2015).

29. Kim, I. & Jabbour, G. E. Effect of annealing on bulk heterojunction organic solar cells based on copper phthalocyanine and perylene derivative. *Synth. Met.* **162**, 102–106 (2012).

30. Shin, W. S. *et al.* Effects of functional groups at perylene diimide derivatives on organic photovoltaic device application. *J. Mater. Chem.* **16**, 384–390 (2006).

31. Qu, J. *et al.* Donor-spacer-acceptor monodisperse conjugated co-oligomers for efficient single-molecule photovoltaic cells based on non-fullerene acceptors. *J. Mater. Chem. A* **2**, 3632–3640 (2014).

32. Lu, Y., Chen, H., Qiao, F., Hu, X. & Ng, S. C. Synthesis, characterization and photovoltaic application of N,N′-bisfluorenyl substituted perylene bisimide. *Sol. Energy Mater. Sol. Cells* **94**, 2036–2041 (2010).

33. Kamm, V. *et al.* Polythiophene:perylene diimide solar cells - The impact of alkyl-substitution on the photovoltaic performance. *Adv. Energy Mater.* **1**, 297–302 (2011).

34. Hartnett, P. E. *et al.* Slip-stacked perylenediimides as an alternative strategy for high efficiency nonfullerene acceptors in organic photovoltaics. *J. Am. Chem. Soc.* **136**, 16345–16356 (2014).

35. Hartnett, P. E. *et al.* Effects of Crystalline Perylenediimide Acceptor Morphology on Optoelectronic Properties and Device Performance. *Chem. Mater.* **28**, 3928–3936 (2016).

36. Li, X. *et al.* Catalyst-free one-step synthesis of ortho-tetraaryl perylene diimides for efficient OPV non-fullerene acceptors. *J. Mater. Chem. C* **5**, 2781–2785 (2017).

37. Sharma, G. D., Balraju, P., Mikroyannidis, J. A. & Stylianakis, M. M. Bulk heterojunction organic photovoltaic devices based on low band gap small molecule BTD-TNP and perylene-anthracene diimide. *Sol. Energy Mater. Sol. Cells* **93**, 2025–2028 (2009).

38. Mikroyannidis, J. A., Suresh, P. & Sharma, G. D. Synthesis of a perylene bisimide with acetonaphthopyrazine dicarbonitrile terminal moieties for photovoltaic applications. *Synth. Met.* **160**, 932–938 (2010).

39. Sharma, G. D., Suresh, P., Mikroyannidis, J. A. & Stylianakis, M. M. Efficient bulk heterojunction devices based on phenylenevinylene small molecule and perylene-pyrene bisimide. *J. Mater. Chem.* **20**, 561–567 (2010).

40. Yi, J. *et al.* Influence of para-alkyl chain length of the bay-phenyl unit on properties and photovoltaic performance of asymmetrical perylenediimide derivatives. *Dye. Pigment.* **126**, 86–95 (2016).

41. Yi, J. *et al.* Molecular geometry regulation of bay-phenyl substituted perylenediimide derivatives with bulky alkyl chain for use in organic solar cells as the electron acceptor. *Dye. Pigment.* **136**, 335–346 (2017).

42. Zhang, X. *et al.* Cooperatively tuning phase size and absorption of near IR photons in P3HT:Perylene diimide solar cells by bay-modifications on the acceptor. *J. Phys. Chem.*

*C* **118**, 24212–24220 (2014).

43. Cheng, P. *et al.* Towards high-efficiency non-fullerene organic solar cells: Matching small molecule/polymer donor/acceptor. *Org. Electron. physics, Mater. Appl.* **15**, 2270–2276 (2014).

44. Kotowski, D. *et al.* The effect of perylene diimides chemical structure on the photovoltaic performance of P3HT/perylene diimides solar cells. *Dye. Pigment.* **120**, 57–64 (2015).

45. Işık Büyükekşi, S. *et al.* Electrochemical, photovoltaic and DFT studies on hybrid materials based on supramolecular self-assembly of a ditopic twisted perylene diimide with square-planar platinum(II)- and/or palladium(II)-2,2′:6′,2″-terpyridyl complex ions. *Dye. Pigment.* **161**, 66–78 (2019).

46. Ma, Z. *et al.* Palladium-Catalyzed Si-C Bond Formation toward Sila-Annulated Perylene Diimides. *Org. Lett.* **19**, 4331–4334 (2017).

47. Choi, H. *et al.* Synthesis of annulated thiophene perylene bisimide analogues: Their applications to bulk heterojunction organic solar cells. *Chem. Commun.* **47**, 5509–5511 (2011).

48. Guo, Y. *et al.* A Vinylene-Bridged Perylenediimide-Based Polymeric Acceptor Enabling Efficient All-Polymer Solar Cells Processed under Ambient Conditions. *Adv. Mater.* 8483–8489 (2016). doi:10.1002/adma.201602387

49. Duan, Y. *et al.* Pronounced Effects of a Triazine Core on Photovoltaic Performance–Efficient Organic Solar Cells Enabled by a PDI Trimer-Based Small Molecular Acceptor. *Adv. Mater.* **29**, 1–6 (2017).

50. Wu, Q., Zhao, D., Schneider, A. M., Chen, W. & Yu, L. Covalently Bound Clusters of Alpha-Substituted PDI-Rival Electron Acceptors to Fullerene for Organic Solar Cells. *J. Am. Chem. Soc.* **138**, 7248–7251 (2016).

51. Liu, J. *et al.* Fast charge separation in a non-fullerene organic solar cell with a small driving force. *Nat. Energy* **1**, (2016).

52. Brebels, J., Manca, J. V., Lutsen, L., Vanderzande, D. & Maes, W. High dielectric constant conjugated materials for organic photovoltaics. *J. Mater. Chem. A* **5**, 24037–24050 (2017).

53. Ramanan, C., Smeigh, A. L., Anthony, J. E., Marks, T. J. & Wasielewski, M. R. Competition between singlet fission and charge separation in solution-processed blend films of 6,13-bis(triisopropylsilylethynyl)pentacene with sterically-encumbered perylene-3,4:9,10-bis(dicarboximide)s. *J. Am. Chem. Soc.* **134**, 386–397 (2012).

54. Zhang, J. *et al.* Intramolecular π-stacked perylene-diimide acceptors for non-fullerene organic solar cells. *J. Mater. Chem. A* **7**, 8136–8143 (2019).

55. Würthner, F. *et al.* Preparation and characterization of regioisomerically pure 1,7-disubstituted perylene bisimide dyes. *J. Org. Chem.* **69**, 7933–7939 (2004).

56. Shi, M. *et al.* Effect of substituents on the aggregate structure and photovoltaic property of violanthrone derivatives. *Dye. Pigment.* **95**, 377–383 (2012).

57. Seybold, G. & Wagenblast, G. New perylene and violanthrone dyestuffs for fluorescent collectors. *Dye. Pigment.* **11**, 303–317 (1989).

58. https://www.ossila.com/products/pbdb-t-pce12?variant=34390460033. (Accessed: 3rd September 2019)

59. Choy, W. C. H. Organic Solar Cells: Materials and Device Physics. *Green Energy Technol.* **128**, (2013).

60. Lee, D., Kim, J., Noh, S. & Lee, C. The thickness of active layer dependence of polymer solar cells. *2010 10th IEEE Conf. Nanotechnology, NANO 2010* 1175–1178 (2010). doi:10.1109/NANO.2010.5698038

61. Li, G., Shrotriya, V., Yao, Y. & Yang, Y. Investigation of annealing effects and film thickness dependence of polymer solar cells based on poly(3-hexylthiophene). *J. Appl. Phys.* **98**, 1–6 (2005).

62. Jiang, Z., Soltanian, S., Gholamkhass, B., Aljaafari, A. & Servati, P. Light-soaking free organic photovoltaic devices with sol-gel deposited ZnO and AZO electron transport layers. *RSC Adv.* **8**, 36542–36548 (2018).

63. Dusza, M., Strek, W. & Granek, F. Significance of light-soaking effect in proper analysis of degradation dynamics of organic solar cells. *J. Photonics Energy* **6**, 035503 (2016).

64. Datt, R. *et al.* Effectiveness of Solvent Vapor Annealing over Thermal Annealing on the Photovoltaic Performance of Non-Fullerene Acceptor Based BHJ Solar Cells. *Sci. Rep.* **9**, 1–10 (2019).

65. Doutora, P. Perylene Diimide acceptors : Fabrication and characterization of electron-only , hole-only devices and solar cells. (2015).

66. Menacher, F. & Wagenknecht, H. A. Synthesis of DNA with green perylene bisimides as DNA base substitutions. *European J. Org. Chem.* 4564–4570 (2011). doi:10.1002/ejoc.201100519

67. Dubey, R. K., Westerveld, N., Grozema, F. C., Sudhölter, E. J. R. & Jager, W. F. Facile synthesis of pure 1,6,7,12-tetrachloroperylene-3,4,9,10-tetracarboxy bisanhydride and bisimide. *Org. Lett.* **17**, 1882–1885 (2015).

68. M. J. Frisch, et al. Gaussian, Inc., Wallingford CT, 2013.